Viscoelastic liquid curtains: Experimental results on the flow of a falling sheet of polymer solution

Antoine Gaillard, Matthieu Roché, Sandra Lerouge, Cyprien Gay, Luc Lebon, Laurent Limat

Viscoelastic liquid curtains: Experimental results on the flow of a falling sheet of polymer solution

Antoine Gaillard[1]†, M. Roché[1] S. Lerouge[1] C. Gay[1] L. Lebon[1] and L. Limat[1]

[1]Laboratoire Matière et Systemes Complexes, CNRS UMR 7057 Université Denis Diderot, 10 rue Alice Domon et Léonie Duquet, 75013 Paris, France

(Received xx; revised xx; accepted xx)

We experimentally investigate the extensional flow of a sheet - or curtain - of viscoelastic liquid falling freely from a slot at constant flow rate under gravity. Extruded liquids are aqueous solutions of flexible polyethylene oxide (PEO) and of semi-rigid partially hydrolysed polyacrylamide (HPAM) with low shear viscosities. Velocimetry measurements reveal that the mean velocity field $U(z)$, z being the distance from the slot exit, does not reduce to a free-fall. More precisely, we show that the liquid falls initially with sub-gravitational accelerations up to a distance from the slot which scales as $g\tau_{fil}^2$, where g is gravity and τ_{fil} is the extensional relaxation time of the liquid, beyond which the local acceleration reaches the asymptotic free-fall value g. The length of the sub-gravitational part of the curtain is shown to be much larger than the equivalent viscous length $((4\eta/\rho)^2/g)^{1/3}$ for Newtonian liquids of density ρ and dynamic viscosity η, which is usually small compared to the length of the curtain. The elastic length $g\tau_{fil}^2$ can indeed be surprisingly large when adding high molecular weight polymer molecules to a low-viscosity Newtonian solvent. By analogy with Newtonian curtains, we show that the velocity field $U(z)$ rescales on a master curve. Besides, we show that the flow is only weakly affected by the history of polymer deformations in the die upstream of the curtain. Furthermore, investigations of the curtain stability reveal that polymer addition reduces the minimum flow rate required to maintain a continuous sheet of liquid.

Key words:

1. Introduction

In extensional flows of polymer solutions, strong elastic stresses may arise due to the stretching of polymer molecules. It has been shown that adding low concentrations of high molecular weight polymer molecules to a low-viscosity Newtonian solvent can indeed significantly modify the structure of the flow, such as in the capillary filament break-up problem (McKinley 2005). The extensional effects of polymer additives are also used to reduce the drag in turbulent pipe flows (Virk 1975), to increase the flow rates of hose streams in firefighting (Chen *et al.* 1998) and to suppress the splashing of droplets impacting on rough solid surfaces in pesticide spraying, spray coating, and inkjet printing (Crooks & Boger 2000).

The influence of elasticity has also been investigated in industrial processes involving free-surface extensional flows such as fibre spinning (Papanastasiou *et al.* 1987) and film casting (Alaie & Papanastasiou 1991; Satoh *et al.* 2001). These techniques aim at producing plastic tubes or sheets respectively. In film casting, a polymer melt is extruded through a slot die and the resulting liquid sheet is cooled before reaching a rotating drum where it is collected. Alaie

† Email address for correspondence: antoine0gaillard@gmail.com

& Papanastasiou (1991) reports that viscoelastic films thin more rapidly at the slot exit than Newtonian films with the same viscosity. The liquids involved in film casting are so viscous that gravity and inertia can generally be neglected since the force exerted by the rotating drum, which stretches the liquid in the flow direction, dominates the process.

Curtain coating is a similar process which aims at depositing a material layer of uniform thickness on a solid surface. It has been intensively investigated on geometries and situations of increasing complexity (Miyamoto & Katagiri 1997). Like in film casting, a simple technique consists in pumping the desired liquid at constant flow rate from a reservoir to a precision head drilled with a long thin slot along its lower face. The sheet - or curtain - of coating liquid falls vertically from the slot before impacting a solid substrate moving horizontally underneath at constant speed. The major difference with film casting is that the liquids involved in curtain coating are generally much less viscous. Therefore, contrary to film casting, the process is dominated by gravity which is now the driving force of the problem.

To date, although the structure of the flow is now well understood in film casting, i.e. in the absence of gravity and inertia, very few authors have addressed the issue of the possible influence of elasticity in the context of curtain coating. The existing works mostly focus on the stability of the sheet. For example, Becerra & Carvalho (2011) and Gugler *et al.* (2010) showed that increasing the apparent extensional viscosity reduces the minimum flow rate required to maintain a stable curtain. Karim *et al.* (2018*b*) recently reported that the curtain flow of low-viscosity polymer solutions with millisecond-scale extensional relaxation times was well captured by a free-fall, i.e. $U = (U_0^2 + 2gz)^{1/2}$ where U is the mean vertical velocity of the liquid, U_0 is the initial velocity at the slot exit, z is the distance from the slot exit and g is the gravitational acceleration. However, to the best of our knowledge, no similar measurements were performed on other solutions with larger relaxation times. Consequently, the influence of elasticity on the curtain flow remains an open question.

In the case of Newtonian liquids however, the structure of the curtain flow is now well documented. Investigations started in the 1960s when Taylor proposed, in the appendix of Brown (1961), the following one-dimensional force balance equation

$$U\frac{\mathrm{d}U}{\mathrm{d}z} = g + \frac{4\eta U}{\rho}\frac{\mathrm{d}}{\mathrm{d}z}\left(\frac{1}{U}\frac{\mathrm{d}U}{\mathrm{d}z}\right), \tag{1.1}$$

where ρ and η are respectively the liquid density and dynamic viscosity. This equation was found to capture the experimental results by Brown (1961). As shown by Aidun (1987) and Ramos (1996), Taylor's equation 1.1 can be derived rigorously from a long-wave approximation of the Navier-Stokes equation using the aspect ratio $a/L_c \ll 1$ as a small parameter where $2a$ and L_c are respectively the slot thickness and the curtain length. The solution of this equation was found by Clarke (1966, 1968). The main result is that viscous dissipation only affects the liquid velocity within a distance from the slot exit which is of order

$$z_v = ((4\eta/\rho)^2/g)^{1/3}, \tag{1.2}$$

("v" for "viscous") with a prefactor which is a decreasing function of the initial velocity U_0 and which is of order 7 for small initial velocities $U_0 \ll \sqrt{gz_v}$ (Brown 1961). The liquid initially falls with sub-gravitational accelerations for $z \ll z_v$, i.e. $U\mathrm{d}U/\mathrm{d}z$ increases with z but is less than g, and finally reaches an asymptotic free-fall regime of constant acceleration g for $z \gg z_v$.

In most experimental and industrial applications involving Newtonian curtains, the length of the sub-gravitational regime is very small compared to the length of the curtain, i.e. $z_v \ll L_c$. Typical orders of magnitude are $z_v = 0.01$ cm for water of viscosity $\eta = 10^{-3}$ Pa.s and $z_v = 1$ cm for pure glycerin of viscosity $\eta = 1$ Pa.s, while the curtain length is typically of order $L_c =$ 10 cm. Hence, for low-viscosity Newtonian liquids, the flow is often approximated by a free-fall.

However, to date, the length of the sub-gravitational regime remains unknown in the case of a viscoelastic curtain. This gap in the literature might lead some authors to assume, incorrectly, that the flow of viscoelastic curtains or jets can be approximated by a free-fall based on the small value of the viscous length z_v.

In this paper, we aim at filling this gap by investigating experimentally the influence of elasticity on the curtain flow. Low-viscosity polymer solutions are extruded from a slot die at constant flow rate and the liquid falls onto a motionless solid surface. We show that the liquid falls with sub-gravitational accelerations up to a distance from the slot which scales as $z_e = g\tau_{fil}^2$ ("e" for "elastic") which happens to be much larger than z_v, where τ_{fil} is the polymer extensional relaxation time. By analogy with Newtonian curtains, we show that the velocity field $U(z)$ rescales on a master curve. Besides, we show that the flow is only weakly affected by the history of polymer deformations upstream of the curtain. We also confirm that adding polymer stabilises the curtain by reducing the minimum flow rate required to maintain a continuous sheet.

This manuscript is organised as follows. First, we present the experimental set-up (§2). Then, we characterise the shear and extensional rheology of the polymer solutions (§3). Next, we turn to the description of the experimental results (§4). Then, after writing down the general force balance equation of the curtain flow, we identify the master curve of the flow by analogy with Newtonian curtains (§5). Next, we investigate the influence of the history of polymer deformations upstream of the curtain (§6). Finally, we discuss the role of elasticity in curtain stability (§7).

2. Materials and methods

2.1. *Polymers and preparation of the solutions*

Experiments are performed with aqueous solutions of two high molecular weight polymers with different rheological behaviours. For each curtain experiment, 5 kg of solution is required.

We use solutions of polyethylene oxide (PEO) of molecular weight $M_w = 8 \times 10^6$ g/mol. The solvent is a Newtonian aqueous solution of polyethylene glycol (PEG) of low molecular weight $M_w = 8000$ g/mol which is used as a thickener (Dontula *et al.* 1998; Becerra & Carvalho 2011; Karim *et al.* 2018*b*). Both polymers are provided by Sigma-Aldrich (refs 372838 and P2139). In most solutions, the PEG concentration is [PEG] = 20 wt% and the corresponding solvent viscosity is $\eta_s = 0.017$ Pa.s. The maximum PEO concentration is 0.4 wt%. A 5 kg solution is prepared by first adding the desired mass of PEO powder to 3 kg of pure water. The solution is shaken for 15 hours to ensure homogeneous mixing. Then, another solution of 1 kg of PEG and 1 kg of water is prepared and the two solutions are mixed. The final solution is shaken for about two hours before use. Following a similar protocol, other solutions are prepared with a higher PEG concentration [PEG] = 40 wt%. The corresponding solvent viscosity is $\eta_s = 0.15$ Pa.s.

We also use solutions of partially hydrolysed polyacrylamide (HPAM), a polyelectrolyte commonly used in oil recovery provided by SNF Floerger (ref Floset 130 VG). Molecular weight is estimated to be around $M_w = 15-20 \times 10^6$ g/mol and the hydrolysis degree is close to 30 %. At equilibrium in water, HPAM molecules are swollen due to repulsive electrostatic charges along the chain backbone and behave as semi-rigid rods, in contrast to PEO molecules which behave as flexible coils. HPAM rigidity can be tuned by adding salt to the solution (Cartalos & Piau 1992). As salt is added, the repulsive interactions are screened and HPAM molecules become more flexible, i.e. their radius of gyration decreases (Chen *et al.* 2012; Zhang *et al.* 2008). In order to investigate the influence of polymer conformation on the curtain flow, we use aqueous solutions of fixed polymer concentration [HPAM] = 0.1 wt% and various salt concentrations [NaCl] ranging between 0 and 10 wt%. A 5 kg solution is prepared by adding 5 g of HPAM

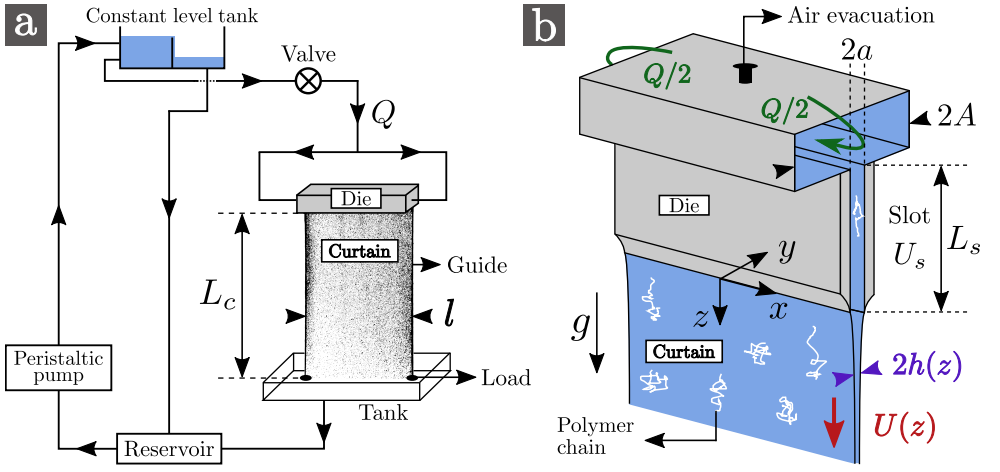

FIGURE 1. Schematic of the hydraulic loop (a) and of the slot die (b).

powder to 5 kg of pure water and shaking for 15 hours to ensure homogeneous mixing. The desired mass of salt is finally added and the final solution is shaken for a few minutes before use.

For a given solvent, density ρ and surface tension γ, which is measured by a pendant drop method (Daerr & Mogne 2016), were found not to depend on polymer concentration. Values are

- $\rho = 1000$ kg/m^3 and $\gamma = 72$ mN/m for HPAM solutions.
- $\rho = 1026$ kg/m^3 and $\gamma = 62$ mN/m for PEO solutions with 20 wt% PEG solvent.
- $\rho = 1070$ kg/m^3 and $\gamma = 53$ mN/m for PEO solutions with 40 wt% PEG solvent.

2.2. *The hydraulic loop*

Most of the curtain experiments were conducted with the hydraulic loop sketched in figure 1.a. The polymer solution is pumped from a reservoir with a peristaltic pump up to a constant level tank, from which it flows down to a slot die by gravity. The liquid then falls vertically from the slot down to a tank, forming a rectangular curtain of width $l = 14.5$ cm and length L_c ranging between 15 cm and up to 200 cm when needed. To avoid sheet retraction due to surface tension, the liquid is guided between two wires (cooking strings) held vertically with loads on the tank surface. The liquid then flows back to the reservoir, thus closing the loop. The liquid mass flow rate Q feeding the die is controlled by a valve and is measured directly by weighing. Q is lower than the flow rate imposed by the pump, and the liquid excess flows directly from the constant level tank to the reservoir. This ensures that the liquid level, and therefore the flow rate, does not vary with time. The constant level tank is about 2 metres above the die. When the valve is completely open, it allows flow rates up to 80 g/s which is the maximum achievable water flow rate of the peristaltic pump. We define the linear flow rate (volumetric flow rate per unit width) as $q \equiv Q/\rho l$. The pulsations caused by the peristaltic pump vanish when the liquid enters the constant level tank, which ensures that the die is fed by a stationary flow.

2.3. *The die*

In figure 1.b we present the geometry of the die. The liquid enters on both sides of a hollow box of width $2A = 14$ mm and then flows through a slot of length $L_s = 10$ cm, width l and thickness $2a = 1$ mm. The contraction ratio is $A/a = 14$. The air inside the die is evacuated using a small hole on top of the box. Once the die is full of liquid, the hole is closed with a screw. The slot consists of two flat walls which were carefully designed to ensure a constant separation distance. The wall edges are bevelled to prevent any wetting of the liquid when leaving the slot. The initial curtain thickness $2h(z = 0)$ is thus expected to be equal to $2a$. Equivalently, the initial

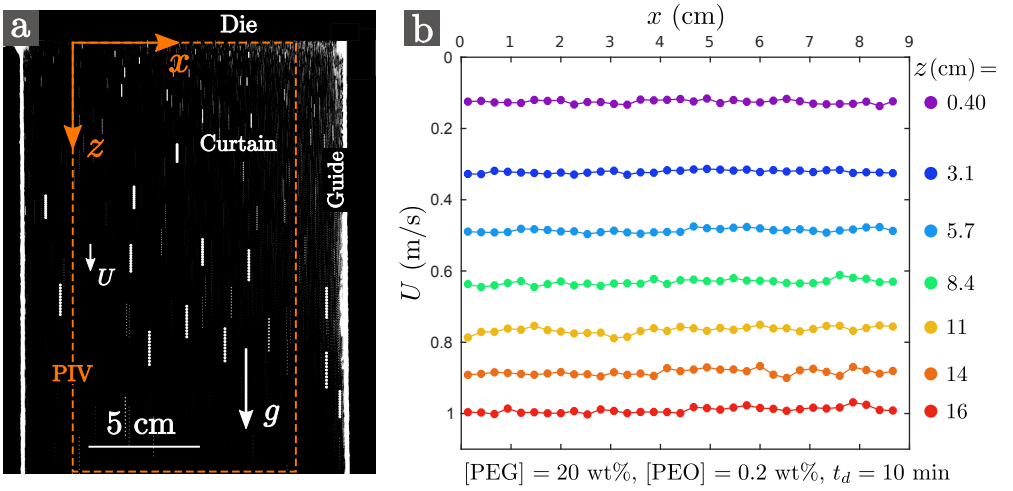

FIGURE 2. Example of PIV measurement for a 0.2 wt% PEO solution with 20 wt% PEG solvent after ten minutes in the hydraulic loop. (a): Superposition of eleven successive PIV images where some tracers are highlighted for clarity. Due to edge effects, the correlation algorithm is applied to a domain restricted to the dashed rectangle. (b): z-component of the velocity field, i.e. $U(x,z,t)$, against the horizontal coordinate x at different distances z from the slot at an arbitrary time t. The curtain length is $L_c = 30$ cm and the linear flow rate is $q = 2.3$ cm^2/s.

mean velocity of the curtain at the slot exit $U_0 \equiv U(z=0)$ is expected to be equal to the mean velocity $U_s = q/2a$ in the slot.

2.4. *Flow visualisation*

We measure the velocity field of the curtain in the $x-z$ plane using the particle image velocimetry (PIV) technique. Polymer solutions are seeded with solid polyamid particles (PSP) of diameter 50 μm and density 1.03 g/cm^3 (provided by Dantec Dynamics) at a concentration of 0.04 wt% corresponding to a volume fraction of 4×10^{-4}. We have checked that these tracers had no influence on the rheology of the solutions. A large-angle objective is mounted on a high-speed camera which records pictures of the curtain at typically 600 frames per second with a typical spatial resolution of 60 pixels per centimetre. The curtain is illuminated with a white continuous light source and cross-correlation is computed over windows of size 16×16 pixels, i.e. typically 2.7×2.7 mm. Note that, due to the finite size of the PIV correlation windows and to some light reflections at the slot exit, the first value $U_1 = U(z_1)$ of the velocity field is measured at a distance $z = z_1 \approx 2.5$ mm below the slot exit. Note that we do not measure the y dependence of the flow field with the technique described in this section.

In figure 2.a, we show a superposition of eleven successive curtain images for a 0.2 wt% PEO solution with 20 wt% PEG solvent. Note that the falling velocity decreases down to 0 when approaching the vertical immobile guides (not visible in figure 2.a). This is the consequence of a boundary layer developing along the flow direction. We measure that our PEO and HPAM curtains are only affected within less than 2 cm from the guides at $z = 20$ cm from the slot. Therefore, the image correlation algorithm is applied to a domain restricted to the dashed rectangle in figure 2.a. This effect is much more pronounced for highly viscous Newtonian liquids. For example, we measure that the boundary layer reaches a size of about 4 cm at $z = 20$ cm for pure glycerin ($\eta \approx 1$ Pa.s), and invades the whole curtain at $z = 10$ cm for honey ($\eta \approx 10$ Pa.s). In the latter case, the velocity field $U(x,z)$ approaches a parabolic shape, i.e. a Poiseuille-like flow in which vertical wires play the role of rigid walls. Such viscous boundary layers are also reported by Karim *et al.* (2018*a*).

Once a curtain is established, images of the flow are recorded during 2 seconds. An example of velocity field obtained by processing a pair of successive images is given in figure 2.b for a 0.2 wt% PEO solution with 20 wt% PEG solvent. We measure that the x component of the velocity field is 0, as expected. Therefore, we plot the z component $U(x,z,t)$ against x for various distances z from the slot at an arbitrary time t. As expected, the flow is fairly independent of x. Therefore, U is averaged along x at each value of z. We obtain $\langle U\rangle_x(z,t)$ which is a function of z and t. Repeating this procedure for different image pairs shows that flow is stationary, as expected since the flow rate is constant. Therefore, $\langle U\rangle_x$ is averaged over 40 image pairs, equally spaced in time and we finally obtain $U(z)\equiv\langle\langle U\rangle_x\rangle_t$. The curtain flow is stationary and translation invariant along x for most of the data presented in this paper. However, some exceptions are observed, as will be investigated in a separate section for clarity (see §4.2).

2.5. *Experimental limitation: the accessible range of flow rates*

For a given liquid, the maximum accessible flow rate Q_{max} feeding the die (when the valve is completely open) can either be determined by the maximum flow rate achievable by the pump (for this liquid) or by the dissipation in the slot. In the latter case, we observe that Q_{max} decreases when increasing the polymer concentration since the liquid viscosity increases. Besides, since the polymer molecules undergo a step strain at the slot entrance, an extra "pressure drop" can arise due to the stretching of polymer molecules, as shown by Rothstein & McKinley (1999) in the case of an axisymmetric contraction. On the other hand, the die has to be fed with a minimum flow rate Q_{min} in order to form a continuous curtain for a reasonable amount of time. We observe that Q_{min} decreases with increasing the polymer concentration, as will be discussed in §7. The resulting range of accessible flow rates $Q_{min}-Q_{max}$ goes from $5-10$ g/s for large polymer concentrations to $20-80$ g/s for low polymer concentrations. In the latter case, the convenient range of flow rates for flow visualisation is closer to $50-80$ g/s since many holes may open in the curtain at low flow rates.

For these reasons, the experiments presented in this manuscript are performed with flow rates Q ranging from 6 g/s for large polymer concentrations to 60 g/s for low polymer concentrations, i.e. the mean velocity $U_s = q/2a = Q/2a\rho l$ in the slot ranges between 0.04 m/s and 0.4 m/s.

3. Rheology of polymer solutions

In this section, we present shear and extensional rheology measurements. Specific solutions were prepared for these purely rheological experiments. PEO solutions with 20 wt% PEG solvent were obtained by dilution of a 0.2 wt% stock solution, except for 0.3 and 0.4 wt% solutions which are prepared independently, while HPAM solutions were obtained by addition of different salt weight fractions to samples of a 0.1 wt% HPAM stock solution. The rheology of the solutions used in curtain experiments, including PEO solutions with 40 wt% PEG solvent, will be presented in a different section for clarity.

3.1. *Shear rheology*

For shear rheology measurements, we use a torque-controlled rheometer (ARES-G2) from TA Instruments equipped with a cone-plate geometry of radius $R_1 = 25$ mm, angle $\theta_1 = 0.04$ rad and truncation gap 0.055 mm. Temperature is controlled by a Peltier device.

Figure 3 shows the shear viscosity η as a function of the shear rate $\dot\gamma$ for PEO and HPAM solutions. The shear rate is decreased from $\dot\gamma_{max}$ to 10^{-3} s^{-1} where $\dot\gamma_{max}$ is as large as possible but is also less than the critical shear rate marking the onset of the elastic flow instability described by Sui & McKenna (2007) where the liquid sample eventually exits the gap. Typically, $\dot\gamma_{max}$ ranges between 100 s^{-1} and 700 s^{-1} for PEO solutions with a large and low concentration respectively.

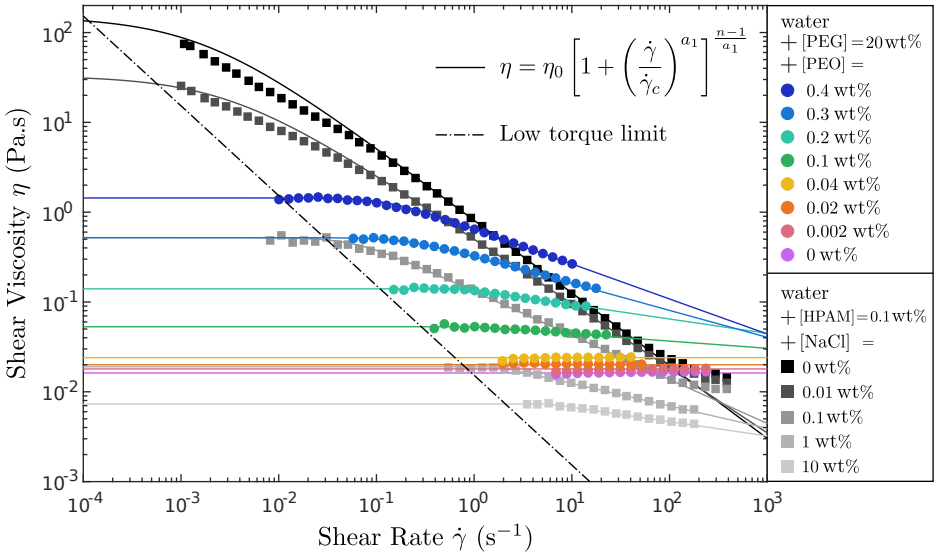

FIGURE 3. Shear viscosity $\eta(\dot\gamma)$ for PEO solutions with 20 wt% PEG solvent and for HPAM solutions at $T = 20°$C. Data are fitted with a Carreau law (equation 3.1). The low-torque limit is shown.

These results are reproducible and are recovered when increasing $\dot\gamma$ from 0 to $\dot\gamma_{max}$. We remove the data below the minimum measurable torque $T_{min} = 0.5$ μN.m, which correspond to $\eta < 3T_{min}/(2\pi R_1^3\dot\gamma)$ (Ewoldt *et al.* 2015). Shear viscosity is fitted by a Carreau law

$$\eta = \eta_0 \left[1 + \left(\frac{\dot\gamma}{\dot\gamma_c}\right)^{a_1}\right]^{(n-1)/a_1}, \tag{3.1}$$

where η_0 is the zero-shear viscosity, $\dot\gamma_c$ is the shear rate at which shear-thinning starts, a_1 is an exponent that encodes the sharpness of the transition and n is the degree of shear thinning. a_1 is always close to 2 and other parameters are presented in table 1.

PEO solutions with 20 wt% PEG solvent behave as Boger fluids, i.e. fluids with constant shear viscosity ($n = 1$), up to [PEO]= 0.04 wt% beyond which shear thinning appears. Shear thinning behaviour is much more pronounced for unsalted HPAM solutions, i.e. when polymer chains are semi-rigid, with $n = 0.19$ for [NaCl]= 0 wt%. The degree of shear thinning is drastically reduced when adding salt. Note that fitting with a Carreau law fails for [NaCl]= 0 wt% and 0.01 wt% and that the Newtonian plateau is beyond the low-torque limit of the rheometer. Therefore, the corresponding values of η_0 reported in table 1 are merely orders of magnitude.

Figure 4 shows the first normal stress difference N_1 as a function of the shear rate $\dot\gamma$. Note that the raw data are corrected by subtracting the negative inertia effects, which tend to pull the plates together, using

$$N_1 = \left(2/\pi R_1^2\right)\left[F_z + 0.075\pi\rho\Omega^2 R_1^4\right], \tag{3.2}$$

where F_z is the total normal force and $\Omega = \tan(\theta_1)\,\dot\gamma$ is the angular velocity (Macosko 1994). PEO chains, due to their flexibility, exhibits more pronounced elastic stresses than HPAM chains. However, although salt addition makes HPAM chains more flexible, it reduces the value of N_1. This can be explained by the fact that normal stresses arise due to both single chain deformability and chain-to-chain interactions. Indeed, since adding salt reduces the radius of gyration of the HPAM chains, polymers are less entangled, resulting in lower normal stresses. In other words,

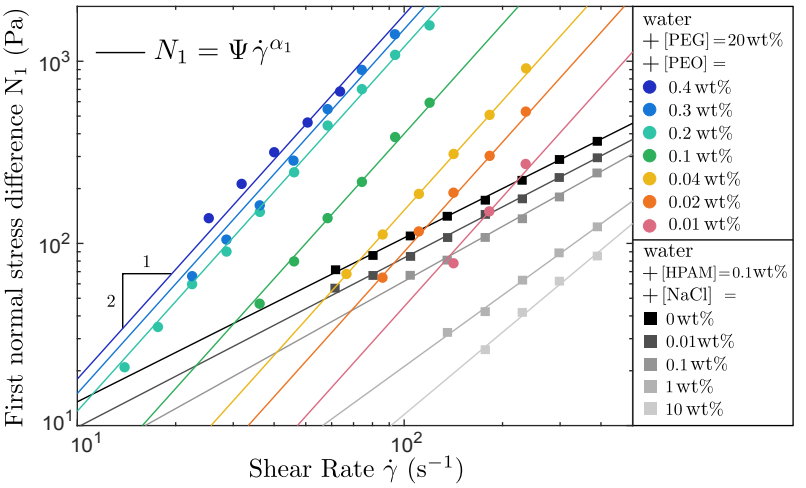

FIGURE 4. First normal stress difference $N_1(\dot{\gamma})$ for PEO solutions with 20 wt% PEG solvent and for HPAM solutions at $T = 20°C$. Data are fitted with a power law (equation 3.3).

the critical overlap concentration increases when adding salt (Chen *et al.* 2012; Zhang *et al.* 2008). The data are fitted with a power law

$$N_1(\dot{\gamma}) = \Psi\dot{\gamma}^{\alpha_1}. \tag{3.3}$$

We find $\alpha_1 = 2$ for PEO solutions. This result is consistent with the Oldroyd-B constitutive model which predicts $N_1 = 2\eta_p\tau\dot{\gamma}^2$ where τ is the relaxation time and $\eta_p = \eta_0 - \eta_s$ is the polymer contribution to the zero-shear viscosity. When $\alpha_1 = 2$, we define a shear relaxation time

$$\tau_{sh} = \Psi/2\eta_0, \tag{3.4}$$

based on η_0 instead of η_p, as suggested by Rothstein & McKinley (1999). For HPAM solutions however, no shear relaxation time can be defined since values of α_1 ranges between 0.90 without salt and 1.5 for [NaCl] = 10 wt%. Values of Ψ, α_1 and τ_{sh} are reported in table 1.

3.2. *Extensional rheology*

Since the curtain flow is an extensional flow, we performed extensional rheology measurements. We use the well documented filament thinning technique described by Anna & McKinley (2001). Our home-made Capillary Breakup Extensional Rheometer (CaBER) is used as follows. A droplet of liquid is placed between two horizontal plates. The lower plate is kept fixed and the upper plate is slowly moved upward until the liquid bridge starts necking. The filament connecting the two end drops undergoes a succession of thinning regimes until final breaking. The process is observed with a high magnification objective (allowing spatial resolution of 1 pixel per micrometre) mounted on a high-speed camera recording up to 1400 images per second. After image processing, we measure the minimum filament radius R as a function of time t.

Figure 5 shows $R(t)$ for PEO and HPAM solutions, along with raw filament images at four stages of thinning. Solutions are tested at room temperature $T = 25°C$ (the effect of temperature will be discussed in §3.5). Each filament undergoes the following steps. First (step 1 in figure 5), the liquid bridge slowly necks due to capillary pressure until abruptly transiting to a slender filament shape (step 2). During this transition, elastic stresses become dominant due to rapid stretching of polymer molecules (Amarouchene *et al.* 2001). The filament then thins exponentially, following

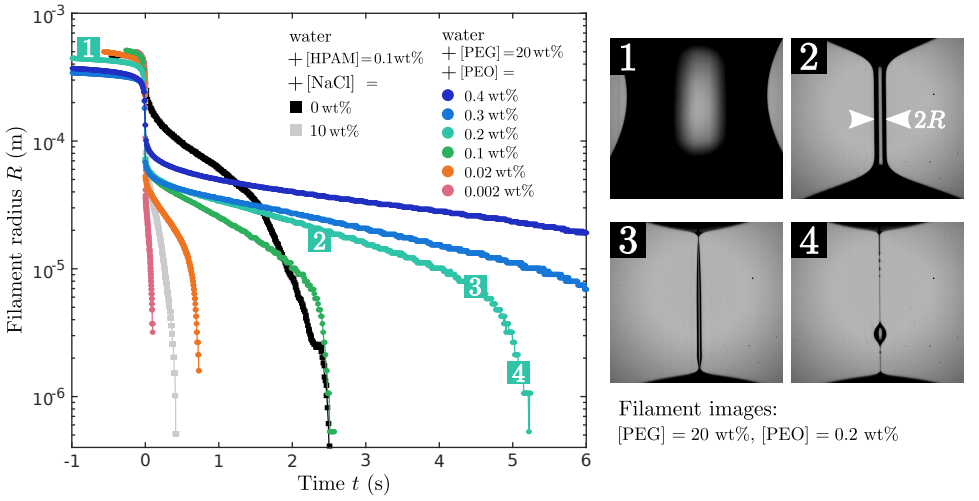

FIGURE 5. Left: minimum filament radius R as a function of time t for PEO solutions with 20 wt% PEG solvent and for HPAM solutions at $T = 25°$C. Right: Four images of a filament of a 0.2 wt% PEO solution during the thinning process. These four steps are reported on the corresponding $R(t)$ curve on the right.

$$R(t) \propto \exp\left(-t/3\tau_{fil}\right). \tag{3.5}$$

We define τ_{fil} as the liquid extensional relaxation time. During this process, the polymer chains undergo progressive unravelling under homogeneous uniaxial elongation flow with constant extension rate $\dot{\varepsilon} \equiv -(2\,\mathrm{d}R/\mathrm{d}t)/R = 2/3\tau_{fil}$. The filament remains perfectly cylindrical since any localised pinching produces additional polymeric stresses which inhibits further pinching. However, when polymer strands have reached their full length, the extensional viscosity reaches a plateau value and the liquid behaves as a Newtonian liquid, allowing local pinching that typically occurs near the end drops (step 3). The filament then undergoes a Rayleigh-Plateau-like instability commonly referred to as "blistering instability" (Sattler *et al.* 2008, 2012; Eggers 2014) where tiny drops are separated by micrometric sub-filaments (step 4). In steps 3 and 4, R refers to the radius of the pinched region and to the radius of the sub-filaments respectively.

Repeating this experiment on different drops of the same liquid shows results which are more reproducible for PEO and salted HPAM solutions than for unsalted HPAM solutions. We found no explanation for this in the literature. Values of τ_{fil} are reported in table 1 with a number of significant digits which reflects the precision of the measurement.

Considering a perfectly cylindrical filament with negligible inertia and gravity, the Laplace pressure γ/R is balanced by both solvent and polymeric stresses. The force balance equation writes $3\eta_s\dot{\varepsilon} + (\sigma_{p,zz} - \sigma_{p,rr}) = \gamma/R$ where $\sigma_{p,zz}$ and $\sigma_{p,rr}$ denote the axial and radial components of polymeric stresses. Defining the apparent extensional viscosity as $\eta_{app} \equiv (\sigma_{zz} - \sigma_{rr})/\dot{\varepsilon} = 3\eta_s + (\sigma_{p,zz} - \sigma_{p,rr})/\dot{\varepsilon}$, it can therefore be estimated using

$$\eta_{app} = -\gamma/\left(2\,\mathrm{d}R/\mathrm{d}t\right). \tag{3.6}$$

Figure 6 shows η_{app} as a function of the total deformation accumulated by fluid elements, which is given by the Hencky strain

$$\varepsilon(t) \equiv \int_0^t \dot{\varepsilon}(t^*)\mathrm{d}t^* = -2\ln\left[R(t)/R_0\right], \tag{3.7}$$

where R_0 is the minimum radius of the bridge when the necking process starts. Models such as the

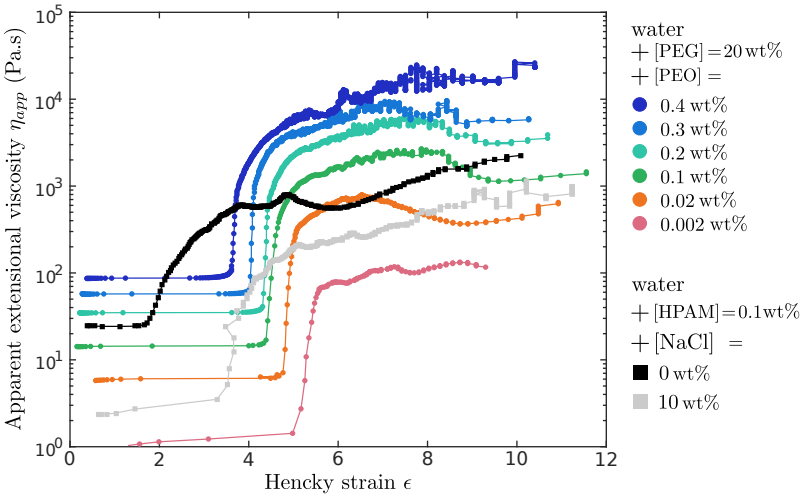

FIGURE 6. Apparent extensional viscosity η_{app} (equation 3.6) as a function of the Hencky strain ε (equation 3.7) for PEO solutions with 20 wt% PEG solvent and for HPAM solutions at $T = 25°$C.

FENE or FENE-P dumbbell models (Bird *et al.* 1987), which include finite polymer extensibility in their description of dilute polymer solutions, predict that η_{app} effectively reaches a plateau value known as the terminal extensional viscosity η_E when polymer chains are fully extended. It can be written as $\eta_E = 3\eta_s + 2b\eta_p$ (McKinley 2005) where $b^{1/2}$ can be seen as the ratio of the polymer length at full extension to its length in the coiled state. Knowing η_s and η_p from shear measurements and η_E from extensional measurements, we can estimate b using $b = (\eta_E - 3\eta_s)/(2\eta_p)$ as a definition. Of course, for semi-dilute solutions, b has to be seen as an effective value since the FENE models does not take into account any chain-to-chain interaction. Values of η_E and b are reported in table 1. The finite extensibility parameter b ranges between 10^3 and 10^5 for flexible PEO and salted HPAM solutions but is only of order 10^0 - 10^1 for semi-rigid unsalted HPAM solutions.

3.3. *Concentration regimes for PEO solutions*

We wish to characterise the different concentrations regimes for PEO solutions with 20 wt% PEG solvent. In the dilute regime, the zero-shear viscosity is expected to be $\eta_0 = \eta_s[1 + [\eta]c + O(c^2)]$ where $c = \rho$[PEO] and $[\eta]$ is the intrinsic viscosity defined as

$$[\eta] = \lim_{c\to 0} \frac{\eta_0 - \eta_s}{c\eta_s}. \tag{3.8}$$

The data of table 1 are indeed well captured by a polynomial law of order 2 for [PEO]$\leqslant 0.2$ wt% (not shown). Curve fitting gives $[\eta] = 0.48$ m^3/kg (equivalently 5.0 wt%$^{-1}$). Using the definition of the critical overlap concentration $c^* = 0.77/[\eta]$ by Graessley (1980), we obtain $c^* = 1.6$ kg/m^3 (equivalently 0.16 wt%) which corresponds to the onset of shear-thinning behaviour.

3.4. *Discussion on the rheological parameters*

Let us now discuss the rheological parameters of table 1. The relaxation times of PEO solutions measured from shear (τ_{sh}) and extensional (τ_{fil}) measurements are in good agreement for [PEO]$\leqslant 0.1$ wt%, i.e in the dilute regime where the shear viscosity is constant. In the theory of Zimm (Tirtaatmadja *et al.* 2006), the relaxation time is

[PEG] wt %	[PEO] wt %	η_0 Pa.s	η_p Pa.s	n	$1/\dot{\gamma}_c$ s	α_1	Ψ Pa.s$^{\alpha_1}$	τ_{sh} s	τ_{fil} s	η_E Pa.s	b
20	0.001	0.017	0.001	1.0					0.009	5×10^1	1×10^4
20	0.002	0.018	0.001	1.0					0.024	2×10^2	7×10^4
20	0.01	0.019	0.002	1.0		2	0.005	0.13	0.080	4×10^2	1×10^5
20	0.02	0.020	0.003	1.0		2	0.009	0.22	0.17	8×10^2	1×10^5
20	0.04	0.024	0.007	1.0		2	0.015	0.31	0.31	2×10^3	1×10^5
20	0.1	0.053	0.036	0.92	1.0	2	0.040	0.38	0.46	3×10^3	4×10^4
20	0.2	0.14	0.12	0.84	1.2	2	0.12	0.43	0.90	6×10^3	2×10^4
20	0.3	0.52	0.50	0.70	5.0	2	0.15	0.14	1.2	1×10^4	1×10^4
20	0.4	1.4	1.4	0.61	7.8	2	0.18	0.064	1.9	2×10^4	5×10^3

[HPAM] wt %	[NaCl] wt %	η_0 Pa.s	η_p Pa.s	n	$1/\dot{\gamma}_c$ s	α_1	Ψ Pa.s$^{\alpha_1}$	τ_{fil} s	η_E Pa.s	b
0.1	0	1×10^2	1×10^2	0.19	6×10^2	0.90	1.7	0.4	1×10^3	3×10^0
0.1	0.01	3×10^1	3×10^1	0.28	3×10^2	0.93	1.2	0.3	8×10^2	1×10^1
0.1	0.1	0.52	0.52	0.51	17	1.0	0.62	0.14	5×10^2	5×10^2
0.1	1	0.019	0.018	0.75	0.56	1.3	0.053	0.064	4×10^2	1×10^4
0.1	10	0.0073	0.0063	0.84	0.17	1.5	0.012	0.057	4×10^2	3×10^4

TABLE 1. Rheological parameters of PEO solutions with 20 wt% PEG solvent (top) and salted (NaCl) HPAM solutions (bottom). Shear parameters: η_0, n, $\dot{\gamma}_c$, α_1 and Ψ are such that the shear viscosity and the first normal stress difference are captured by equations 3.1 and 3.3. $\eta_p = \eta_0 - \eta_s$ where η_s is the solvent viscosity which is respectively 0.017 Pa.s (top) and 0.001 Pa.s (bottom). τ_{sh} is the shear relaxation time defined in equation 3.4. Extensional parameters: τ_{fil} is the extensional relaxation time and η_E is the terminal extensional viscosity. $b = (\eta_E - 3\eta_s)/(2\eta_p)$ is the effective value of the finite extensibility parameter.

$$\tau_Z = \frac{1}{\zeta(3\nu)}\frac{[\eta]M_w\eta_s}{\mathcal{N}_A k_B T}, \tag{3.9}$$

where ζ is the Riemann zeta function, $\mathcal{N}_A$ is Avogadro's number, k_B is the Boltzmann constant and ν is such that the equilibrium radius of gyration R_g of the polymer chain scales with molecular weight as $R_g \propto M_w^\nu$. The limiting values are $\nu = 1/2$ in theta solvent and $\nu = 3/5$ in good solvent. Assuming $\nu = 0.55$ for PEO (Tirtaatmadja *et al.* 2006), the prefactor is $1/\zeta(1.65) \approx 0.463$ and we obtain $\tau_Z = 0.012$ s which is in agreement with the values of τ_{fil} for very dilute PEO solutions. The discrepancy between τ_Z and τ_{fil} in the dilute regime ($c < c^*$) can be explained by polymer chain-to-chain interactions during the filament thinning process. Indeed, since the extension rate $\dot{\varepsilon}$ is such that $\tau_{fil}\dot{\varepsilon} = 2/3$, which is larger than the coil-stretch transition value $1/2$, the polymer chains occupy a much larger effective volume than at equilibrium (Clasen *et al.* 2006; Tirtaatmadja *et al.* 2006).

Some scalings can be extracted from the data of table 1. The PEO extensional relaxation time is well captured by $\tau_{fil} = 3.7\,(100\,[\mathrm{PEO}])^{0.84}$. The exponent 0.84 is consistent with Zell *et al.* (2010). According to Stelter *et al.* (2002), the terminal extensional viscosity η_E is proportional to τ_{fil} with a prefactor which is larger for flexible polymers than for rigid polymers. Our data indeed suggests $\eta_E = E\,\tau_{fil}$ with $E \approx 8\times10^3$ Pa for solutions of flexible chains such as PEO and salted HPAM, whereas E is closer to 2.5×10^3 Pa for solutions of semi-rigid chains such as unsalted HPAM. The data of table 1 also suggests a link between the degree of shear-thinning n and the effective value of the finite extensibility parameter b. Indeed, solutions of flexible polymers

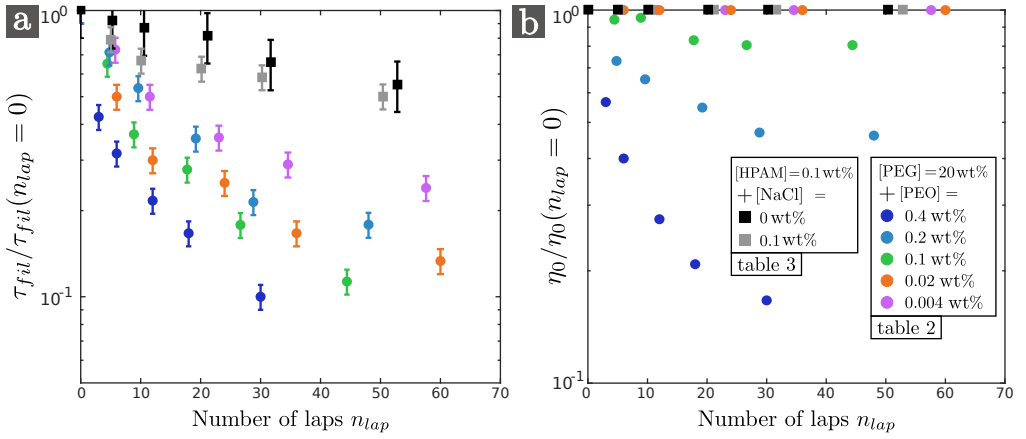

FIGURE 7. Dependence of the extensional relaxation time τ_{fil} (a) and of the zero-shear viscosity η_0 (b) on the number of laps n_{lap} through the hydraulic loop for PEO solutions with 20 wt% PEG solvent (table 2) and for HPAM solutions (table 3 (top)). n_{lap} is estimated by $t_d Q/M$ where t_d is the time spent since the start of the experiment, Q is the mass flow, and $M = 5$ kg is the mass of the solution. For each liquid, τ_{fil} and η_0 are normalised by the initial values before degradation, i.e. at $t_d = 0$.

correspond to large values of b with n close to 1 while shear-thinning solutions correspond to low values of b. For both PEO and HPAM solutions we find the following empirical formula: $n \approx 0.16 b^{0.17}$ for $b < 5 \times 10^4$ and $n = 1$ for $b \geqslant 5 \times 10^4$.

3.5. *Mechanical degradation of polymer chains and adequate protocols*

During sample preparation (see §2.1), degradation of the polymer chains may occur during shaking. This is particularly true for PEO solutions since we measured that the relaxation time of two independently prepared solutions of same PEO concentration could vary by a factor of up to 4. Hence, the rheological data presented in the previous sections which correspond to specific solutions with a particular preparation history can not be used as a reference for all other solutions. Therefore, rheological measurements are performed on any newly prepared solution. Nevertheless, the data presented in the previous sections capture the main trends and orders of magnitude. In particular, the scalings found in §3.4 remain true.

Mechanical degradation of the polymer chains also occur in the hydraulic loop described in §2.2. Indeed, in this closed-loop system, polymer chains flow many times through the peristaltic pump which was found to be the principal source of degradation. Since irreversible scission of the polymer molecules occurs at each passage through the pump, the rheological properties of the solution varies with time. Therefore, it would be incorrect to correlate curtain data with the rheological properties of the initial fresh solutions. In order to overcome this problem, we use two different experimental protocols.

For the first protocol, we take advantage of degradation by proceeding as follows. A newly prepared solution is placed in the reservoir and the pump is turned on at time $t_d = 0$. Filling the loop and setting the desired flow rate takes about 1 minute. A first PIV measurement is performed, and we immediately collect a sample of the solution from the die. Without changing any external parameter, this procedure is repeated at times $t_d = 10$, 20, 40, 60 and 100 minutes. We therefore obtain six velocity profiles $U(z)$ corresponding to six degradation degrees of a given initial solution, which can be unambiguously correlated to the rheological properties of the six corresponding samples. For simplicity, the solution corresponding to the first measurement is called the fresh solution and is referred to as $t_d = 0$. Note that the flow rate Q has to be regularly readjusted because it increases naturally over time due to a decreasing dissipation in the slot.

For a solution of total mass $M = 5$ kg flowing with mass flow Q, the number of laps through the loop is $n_{lap} \approx t_d Q/M$ where t_d is the time spent since the start of the experiment. We show in figure 7 the extensional relaxation time τ_{fil} (a) and the zero-shear viscosity η_0 (b) as a function n_{lap} for PEO solutions with 20 wt% PEG solvent and for HPAM solutions. Values at time $t_d = 0$, 10, 20, 40, 60 and 100 minutes are normalised by the initial value before degradation, i.e. at $t_d = 0$. Since the solutions are extruded at different flow rates (see §2.5), the values reported in figure 7 correspond to different values of n_{lap}. For PEO solutions, τ_{fil} decreases by a factor of up to 10 after 100 minutes of circulation. In contrast, HPAM chains are more resistant since they deteriorate at a much lower rate. Besides, we observe that η_0 only decreases for PEO solutions which exhibit shear-thinning behaviour.

The detailed rheological parameters of all the solutions presented in figure 7 are summarised in tables 2 and 3 (top). Shear thinning PEO solutions become less shear thinning during degradation, i.e. n increases. Note that an extra HPAM solution is presented in table 3 (bottom): starting from a fresh unsalted HPAM solution, five PIV measurements are performed at arbitrary times, each measurement corresponding to a particular salt concentration which is achieved by adding a particular salt quantity to the solution. Samples are again collected at each step and shear and extensional rheological measurements are performed on each sample. Since polymer degradation is slow for HPAM solutions, we ensure that the drastic modifications of the rheological parameters reported table 3 (bottom) are mostly due to salt addition.

A second protocol is used when investigating the role of external parameters such as the curtain length (§4.3), the flow rate (§4.4) or the die geometry (§6.3). In this case, solutions must have the exact same rheological properties for each measurement. Instead of using the peristaltic pump, the liquid is poured manually from a bucket directly into a tank placed at two metres above the die and drilled with a hole on the lower side. A constant flow rate is ensured by keeping a constant liquid level in the tank. With 5 kg of liquid, this protocol is only possible if the time to perform a controlled experiment is less than the time to empty the bucket. This degradation-free protocol was used with the PEO solutions with 40 wt% PEG solvent presented in table 4, which correspond to almost Boger fluids ($n \approx 1$) with large extensional relaxation times, and with the PEO solution of table 5. We checked that the shear and extensional rheological parameters do not vary during experiments.

Curtain experiments are performed at room temperature, which could vary between 20°C and 30°C from day to day. Since temperature is not imposed in our home-made CaBER rheometer, the extensional rheology measurements are always performed a few minutes after curtain experiments and in the same room. Extensional parameters are therefore expected to faithfully reflect the rheological properties of the curtain liquid. For the liquids of tables 4 and 5, the temperature of the curtain room was imposed for shear rheology measurements. However, for the liquids of tables 2 and 3, shear rheology measurements were performed at a temperature $T = 20$°C which was not necessarily the room temperature. We measured on similar solutions that the variation of the viscosity parameters η_0, n and $\dot{\gamma}_c$ is very weak within this temperature range. The zero-shear viscosity η_0 typically decreases by a factor of only 1.1 when raising the temperature from 20°C to 30°C, while n and $\dot{\gamma}_c$ remain unchanged. Hence, we can reasonably use the 20°C values reported in tables 2 and 3. In contrast, the variation of the first normal stress difference parameters is not negligible, i.e. Ψ typically decreases by a factor of 2 when raising the temperature from 20°C to 30°C while α_1 is unchanged. Therefore, the values of Ψ reported in tables 2 and 3 are only acceptable orders of magnitude. In fact, as we shall see in the next sections, Ψ is irrelevant for the discussions concerning these particular solutions. However, for questions regarding the first normal stress difference such as die swell (§4.6 and §6.1) and the impact of die geometry on the curtain flow (§6.3), we make sure that shear rheology measurements are performed at the same temperature as the curtain experiments.

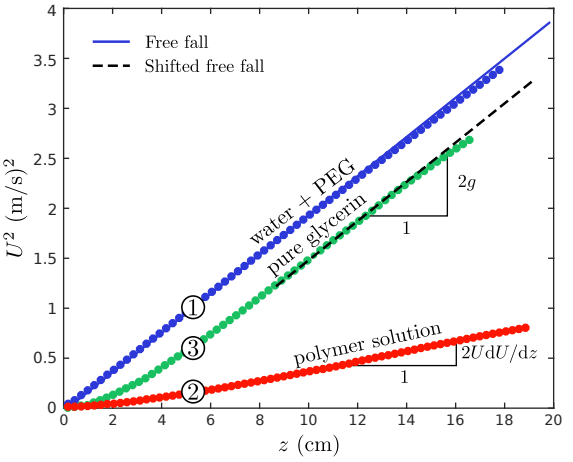

FIGURE 8. Square U^2 of the falling velocity as a function of the distance z from the slot for two Newtonian curtains (1) and (3), a 20 wt% PEG solution and pure glycerin of viscosities $\eta = 0.017$ Pa.s and $\eta = 1.5$ Pa.s respectively, and for a fresh ($t_d = 0$ min) 0.2 wt% PEO solution (2) with 20 wt% PEG solvent of zero-shear viscosity $\eta_0 = 0.12$ Pa.s (table 2). The curtain length is $L_c = 30$ cm and the initial velocity U_1 at $z_1 \approx 2.5$ mm from the slot exit is 0.2 m/s, 0.13 m/s and 0.07 m/s for liquids (1), (2) and (3) respectively. The local acceleration of the liquid is $U\mathrm{d}U/\mathrm{d}z$.

4. Observations

4.1. *A dramatic shift towards sub gravity accelerations*

To identify the specificity of polymer solutions in the context of curtain flows, we have performed a first serie of experiments with three different liquids. The first one (1) is the Newtonian 20 wt% PEG solvent of viscosity $\eta = 0.017$ Pa.s (see §2.1). The second one (2) is a fresh ($t_d = 0$ min) 0.2 wt% PEO solution with 20 wt% PEG solvent (table 2). Its zero-shear viscosity is $\eta_0 = 0.12$ Pa.s, ten times larger than the pure solvent (1). The third one (3) is pure glycerin, a Newtonian liquid with a measured viscosity $\eta = 1.5$ Pa.s, a hundred times larger than the shear viscosity of liquid (1), and density $\rho = 1250$ kg/m^3. Note that we used a different setup for glycerin since, due to a strong viscous dissipation in the hydraulic loop, the maximum accessible flow rate is well below the minimum flow rate required to create a continuous curtain. Glycerin is placed in a reservoir connected to the die and a large enough flow rate is enforced by applying a constant air flow on the top of the reservoir.

In figure 8, we plot the square U^2 of the falling velocity of these liquids as a function of the distance z from the slot. All three curtains have the same length $L_c = 30$ cm and start from comparable initial velocities U_1 ranging between 0.07 m/s for glycerin (3) and 0.2 m/s for the PEG solvent (1). We recall that $U_1 = U(z_1)$ is the liquid velocity at $z_1 \approx 2.5$ mm from the slot exit (see §2.4) while $U_0 = U(z = 0)$ is the liquid velocity at the slot exit. The local acceleration of the liquid is given by $U\mathrm{d}U/\mathrm{d}z$ which is half the local slope of the $U^2(z)$ curve. For both Newtonian curtains (1) and (3), we observe that this acceleration is equal to g far from the slot exit. More precisely, the fall of the low-viscosity Newtonian liquid (1) is very well captured by a free-fall, i.e. $U^2 = U_0^2 + 2gz$, whereas the acceleration of glycerin reaches the asymptotic value g at about 10 cm from the slot. These results are in agreement with the theory of viscous Newtonian curtains (equation 1.1) according to which viscous forces are negligible far downstream from the slot. Indeed, the length of the sub-gravitational part of the flow is of order $z_v = ((4\eta/\rho)^2/g)^{1/3}$ (equation 1.2), respectively 0.077 cm and 1.4 cm for liquids (1) and (3), with a prefactor which is about 7 for low initial velocities $U_0 \ll \sqrt{gz_v}$ (Brown 1961; Clarke 1968). In particular, we measure $U_0 = 0.05$ m/s from the glycerin curtain movie, which gives $U_0/\sqrt{gz_v} \approx 0.14 < 1$.

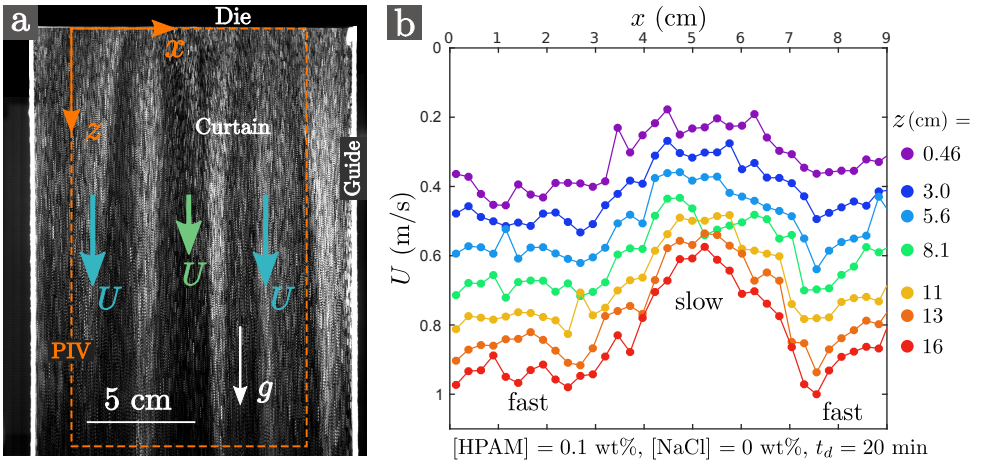

FIGURE 9. Example of PIV measurement for a degraded ($t_d = 20$ min) 0.1 wt% unsalted HPAM solution (table 3). (a): Superposition of six successive PIV images. The correlation algorithm is applied to a domain restricted to the dashed rectangle. (b): z-component of the velocity field, i.e. $U(x,z,t)$, against the horizontal coordinate x at different distances z from the slot at an arbitrary time t. The curtain length is $L_c = 30$ cm and the linear flow rate is $q = 3.1$ cm^2/s.

Hence, according to the theory, the length of the sub-gravitational part of the flow should be about $7\,z_v \approx 10$ cm which is in agreement with the experimental results.

In contrast, the PEO solution falls at much lower velocities than the two others, despite the fact that its zero-shear viscosity is one order of magnitude smaller than the viscosity of glycerin. More precisely, the acceleration at $z = 14$ cm from the slot is $U\mathrm{d}U/\mathrm{d}z = 2.5$ m/s$^2 < g$ despite the fact that the viscous length $z_v = ((4\eta_0/\rho)^2/g)^{1/3}$ is only 0.28 cm based on the zero-shear viscosity. Therefore, viscoelastic curtain flows are not captured by the Newtonian curtain theory.

4.2. *Unstable flow for the most shear-thinning solutions*

We observed that the curtain flow is not always stationary and translation invariant in the x horizontal direction as displayed in figure 9. Indeed, for some solutions, the curtain flow is unstable and presents a time-dependent varicose mode along x. More precisely, at a given time, the extrusion velocity of the liquid is found to depend on the position x along the slot, producing a modulation of the thickness of the curtain. This is illustrated by the vertical dark and bright stripes in figure 9.a for an unsalted HPAM solution. This is one of the most extreme cases of unstable curtain flow. The wavelength and the typical time of evolution of the pattern are of the order of a few centimetres and a few tens of seconds respectively. The corresponding velocity field $U(x,z,t)$ is presented in figure 9.b at an arbitrary time t. The dark and bright stripes are associated with flow regions with characteristic velocities respectively slower and faster than the average velocity. For example, at a distance $z = 16$ cm from the slot, the liquid velocity ranges between 0.6 m/s and 1 m/s which corresponds to a variation of $\pm 25\%$ around the average value $\langle U\rangle_x = 0.85$ m/s. The time variation of the average velocity $\langle U\rangle_x$ is presented in figure 10.a: it is fairly independent of time. Hence, we can reasonably define an average flow $U(z) = \langle\langle U\rangle_x\rangle_t$ obtained after averaging $\langle U\rangle_x$ over time, as presented in figure 10.b.

As salt is added to an initially unsalted HPAM solution, the amplitude of the instability decreases. For the HPAM solutions of table 3 (bottom), the amplitude of the velocity variation is $\pm 25\%$ without salt, it decreases down to $\pm 15\%$ for [NaCl] $= 0.1$ wt% and the instability disappears for [NaCl] $\geqslant 1$ wt%. Besides, for PEO solutions with 20 wt% PEG solvent (table 2), the curtain flow is weakly unstable for the highest concentration [PEO] $= 0.4$ wt%. Before degradation ($t_d = 0$ min), the liquid velocity ranges between 0.23 m/s and 0.29 m/s at a distance

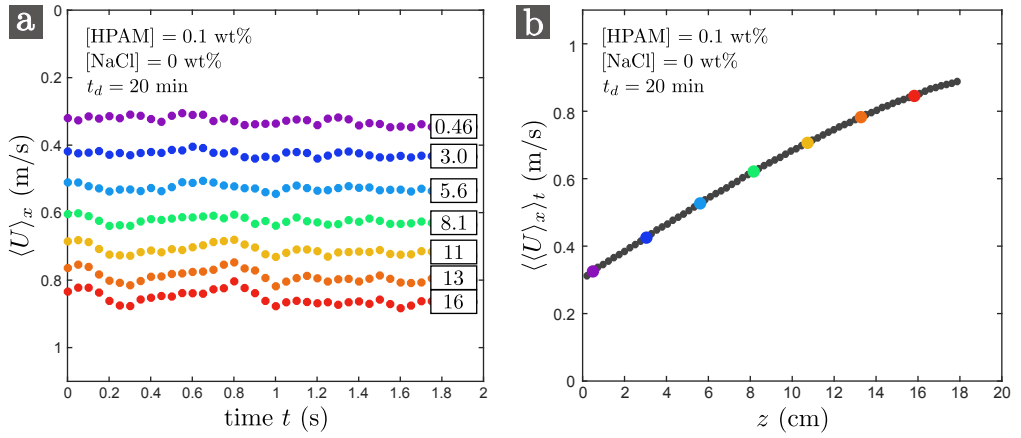

FIGURE 10. (a): Velocity $\langle U \rangle_x$ averaged over x versus time t (for a two seconds PIV movie) and at different distances z from the slot. Time $t = 0$ s corresponds to the data of figure 9.b. (b): Velocity $\langle\langle U \rangle_x \rangle_t$ averaged over x and t versus z. The big coloured dots correspond to the values of figure a.

$z = 16$ cm from the slot, which corresponds to a variation of $\pm 13\%$ around the mean value. As the polymer chains break due to mechanical degradation, the amplitude of the velocity variation decreases: it is typically $\pm 12\%$ for $t_d = 10$ min, $\pm 4\%$ for $t_d = 20$ min, and the instability disappears for $t_d \geqslant 40$ min. All other solutions in table 2 produce a stable curtain. Finally, every PEO solutions with 40 wt% PEG solvent (table 4) produces a stable curtain.

Within our experimental range of rheological parameters and flow rates, the only solutions producing an unstable flow have a degree of shear-thinning $n < 0.70$ or, equivalently, an effective finite extensibility $b < 2 \times 10^3$. Neither the zero-shear viscosity η_0 nor the extensional relaxation time τ_{fil} does provide such a clear separation between stable and unstable curtains. According to preliminary visualisations, this instability appears to be generated at the contraction flow upstream from the slot. A more complete description and characterisation of this instability is left for a future work. In this paper, whatever the curtain, stable or unstable, we focus on the mean flow $U(z) = \langle\langle U \rangle_x \rangle_t$.

4.3. *The influence of the curtain length*

To investigate the role of the curtain length L_c on the flow, we perform experiments with L_c ranging from 15 cm to 200 cm. The experimental set-up is modified: after extrusion, the liquid is stopped at the desired distance L_c from the slot by a 20×10 cm horizontal plastic plate and finally falls into a reservoir. The vertical wires guiding the flow pass through two small holes drilled on the plastic plate to ensure that all the liquid is stopped. The camera only records the first 32 centimetres of the fall. Only the most elastic solutions could form a 2 meters continuous curtain. On the other hand, curtains made of solutions with low polymer concentration usually break before reaching the plastic plate. Near the breaking zone, some curtains may even adopt a sinuous flag-like motion. We suspect that this is due to the shear instability with the surrounding air described by Dombrowski & Johns (1963) and Villermaux & Clanet (2002).

For these experiments, we use the PEO solutions with 40 wt% PEG solvent presented in table 4 along with the degradation-free protocol presented in §3.5 to ensure that L_c is the only varying parameter for a given solution. We only consider the curtains reaching the plastic plate without breaking. Some results are presented in figure 11 for [PEO] = 0.2 wt% (a) and [PEO] = 0.024 wt% (b). In the first case, longer curtains fall clearly faster than shorter ones, i.e. the velocity U is larger at a any distance z from the slot. The liquid vertical velocity has to vary from the imposed initial velocity $U(0) = U_0$ at the slot exit to $U(L_c) = 0$ when impinging onto

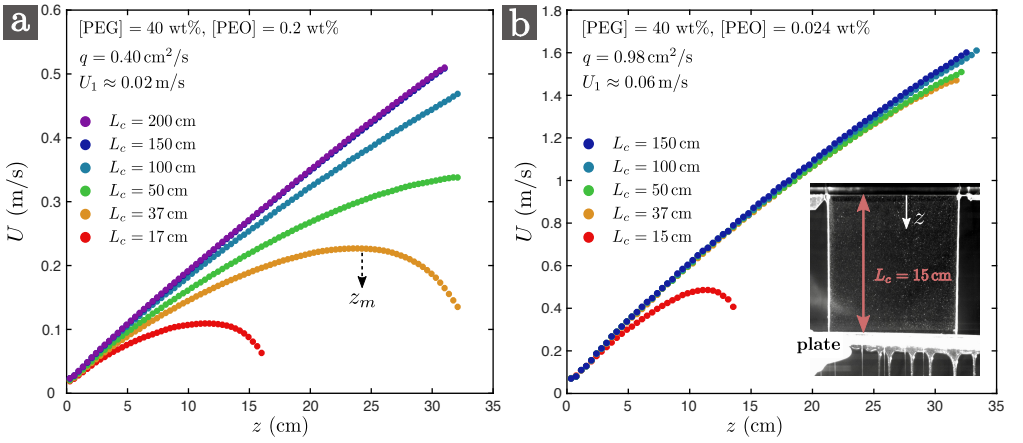

FIGURE 11. Velocity field $U(z)$ for $z \leqslant 32$ cm for curtains of lengths L_c ranging between 15 cm and 200 cm. The liquid falls onto a motionless horizontal plate (see inset on the right) and reaches a maximum velocity at a distance z_m from the slot. The liquids are respectively 0.2 wt% (a) and 0.024 wt% (b) PEO solutions with 40 wt% PEG solvent (table 4). They are respectively extruded at flow rates $q = 0.40$ cm^2/s and 0.98 cm^2/s. The liquid velocity U_1 at $z_1 \approx 2.5$ mm from the slot is respectively 0.02 m/s and 0.06 m/s.

the motionless plastic plate where the curtain flow turns into a plane stagnation flow. Everyday experience with jets of tap water suggests that the presence of a horizontal solid surface only affects the liquid flow within a few millimetres before impact. However, for the liquid of figure 11.a with extensional relaxation time $\tau_{fil} = 1.1$ s, the presence of the plate clearly affects the flow on a much larger scale: for $L_c = 37$ cm, the liquid velocity first increases and reaches a maximum value at $z = z_m \approx 25$ cm before decreasing, i.e. the curtain starts to get thicker at a distance $L_c - z_m \approx 12$ cm from the impact. As the plate is moved downwards, the flow field near the slot exit converges towards a universal behaviour which is no longer influenced by the presence of the plate: there is no difference between $L_c = 150$ cm and $L_c = 200$ cm within the first 32 centimetres of the fall in figure 11.a. This is even more visible for the solution used in figure 11.b which has a lower extensional relaxation time $\tau_{fil} = 0.17$ s since the liquid velocity $U(z)$ is almost the same for all curtain lengths, except for $L_c = 15$ cm.

4.4. *The influence of the flow rate*

To investigate the role of the flow rate, we perform experiments using the degradation-free protocol presented in §3.5 to ensure that q is the only varying parameter for a given solution. The test liquid is the PEO solution presented in table 5 which is close to (but not exactly the same as) the degraded ($t_d = 100$ min) 0.4 wt% PEO solution with 20 wt% PEG solvent presented in table 2. The liquid is extruded at different flow rates q ranging between 0.45 cm^2/s and 1.4 cm^2/s. In figure 12.a, we report the velocity field $U(z)$ for these two flow rates. U increases slightly faster when increasing the flow rate. To quantify this effect, values of the liquid acceleration $U\mathrm{d}U/\mathrm{d}z$ at an arbitrary distance $z = 16$ cm from the slot are reported in figure 12.b as a function of the initial velocity U_1 measured at $z \approx 2.5$ mm from the slot exit.The local acceleration is increased by a factor 1.2 when U_1 is increased by a factor 1.7. The same trend is observed for all solutions, including HPAM solutions (results not shown).

4.5. *The influence of the rheological properties*

To investigate the role of the rheological properties, we show in figure 13.a the square $U^2(z)$ of the velocity field for the six 0.1 wt% PEO solutions with 20 wt% PEG solvent presented in table 2. These measurements are performed with the degradation protocol presented in §3.5 and

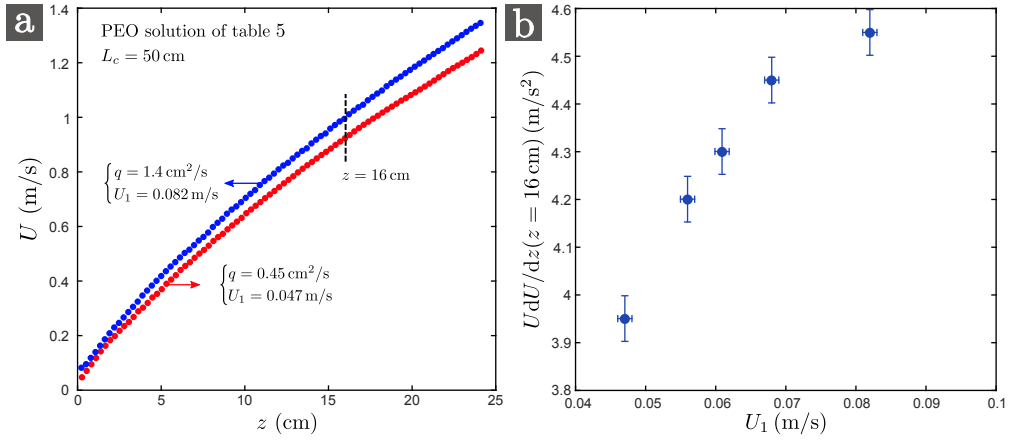

FIGURE 12. (a): Velocity field $U(z)$ for the PEO solution of table 5 extruded at flow rates $q = 0.45$ cm^2/s and 1.4 cm^2/s. The liquid velocity U_1 at $z_1 \approx 2.5$ mm from the slot is respectively 0.047 m/s and 0.082 m/s. (b): Local acceleration $U\mathrm{d}U/\mathrm{d}z$ at an arbitrary distance $z = 16$ cm from the slot versus initial velocity U_1. The curtain length is $L_c = 50$ cm.

each solution corresponds to a specific degradation time. The liquid initial velocity is about $U_1 \approx 0.17$ m/s at $z_1 \approx 2.5$ mm from the slot for all six solutions and the curtain length is $L_c = 30$ cm. Despite the fact that all six solutions almost behave as Boger fluids ($n \approx 0.96$) with similar zero-shear viscosities $\eta_0 \approx 0.03$ Pa.s, we observe that the liquid velocity increases much faster for degraded solutions. The same conclusion can be drawn for the 0.02 wt% and 0.004 wt% PEO Boger solutions with 20 wt% PEG solvent presented in table 2 (results not shown), although their shear viscosity is not affected at all by degradation. This result suggests that the zero-shear viscosity is mostly irrelevant for the description of the curtain flow. It is not surprising since the flow is essentially an extensional plug flow far from the slot, and extensional parameters are probably more relevant than shear parameters. This distinction is avoided for Newtonian curtains since the dynamic viscosity η is relevant in both shear and extensional flows.

In figure 13.b, we plot the square $U^2(z)$ of the velocity field for various PEO and HPAM solutions from tables 2 and 3 (bottom). The curtain length is $L_c = 30$ cm and we choose five pairs of solutions such that both solutions within each pair share comparable extensional relaxation times τ_{fil} and initial velocities U_1. The results suggest that the liquid fall is mostly influenced by the value of τ_{fil} since the flow of both solutions within each pair is very similar. More precisely, the flow of solutions (1), which have low extensional relaxation times $\tau_{fil} = 7 - 8$ ms, is well captured by a free fall with constant acceleration $g = 9.81$ m/s^2, whereas other solutions with larger values of τ_{fil} fall with sub-gravitational accelerations. In the latter case, note that the local acceleration $U\mathrm{d}U/\mathrm{d}z$ is an increasing function of z. These results are consistent with the recent results of Karim *et al.* (2018*b*) who also measured free-falls for curtains made of PEO solutions with extensional relaxation times $\tau_{fil} \leqslant 7.3$ ms.

Note that the shear rheology is not necessarily the same within each pair in figure 13.b, especially when comparing the PEO and HPAM solutions of pair (3) which have different values of α_1 and η_0, i.e. different first normal stress differences and different shear viscosities. This example reinforces the idea that shear parameters are irrelevant for the description of the curtain flow. Besides, the flexibility of the polymer chains do not seem to have a huge effect on the flow since the values of the effective finite extensibility b and of the degree of shear-thinning n are very different for the solutions of pair (5). To confirm these ideas, we gather all the data corresponding to $L_c = 30$ cm in figure 14 where the acceleration at a given (arbitrary) distance $z = 18$ cm from the slot is plotted against τ_{fil}. We observe a good collapse of the data although neighbouring

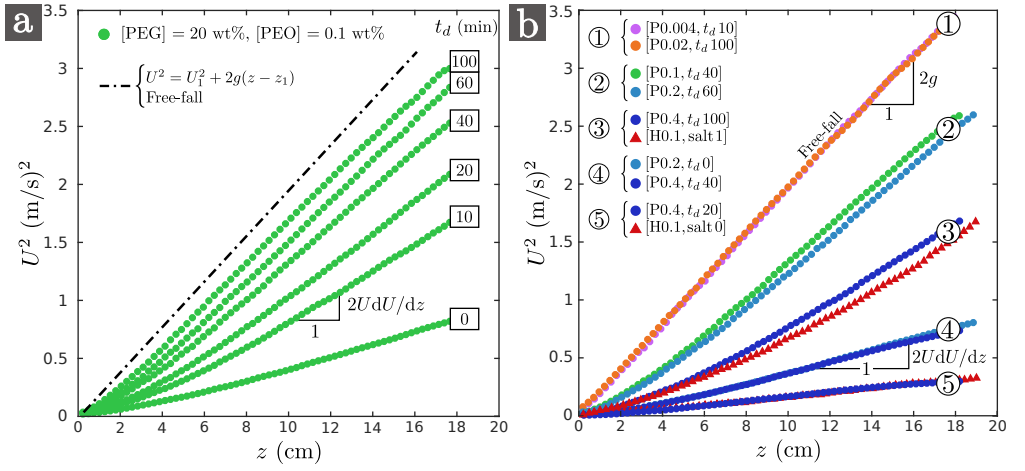

FIGURE 13. Dependence of the velocity field $U(z)$ on the rheological properties of the solution. (a): $U^2(z)$ for the 0.1 wt% PEO solutions with 20 wt% PEG solvent (table 2) for all degradation times $t_d = 0$ to 100 min. All solutions are almost Boger fluids of comparable zero-shear viscosity $\eta_0 \approx 0.03$ Pa.s and have comparable initial velocities $U_1 \approx 0.17$ m/s at $z_1 \approx 2.5$ mm from the slot. A free-fall is shown for comparison. (b): $U^2(z)$ for five pairs of solutions (1), (2), (3), (4) and (5) from tables 2 and 3 (bottom) which are referred to as follows: [P0.2, t_d 60] corresponds to a 0.2 wt% PEO solution (with 20 wt% PEG solvent) with degradation time $t_d = 60$ min and [H0.1, salt 1] corresponds to a 0.1 wt% HPAM solution with salt concentration [NaCl] = 1 wt%. Within each pair, both solutions share similar initial velocities U_1 and comparable extensional relaxation times ranging between $\tau_{fil} = 0.0073 - 0.008$ s (1) to $\tau_{fil} = 0.38 - 0.5$ s (5). The curtain length is $L_c = 30$ cm for both figures.

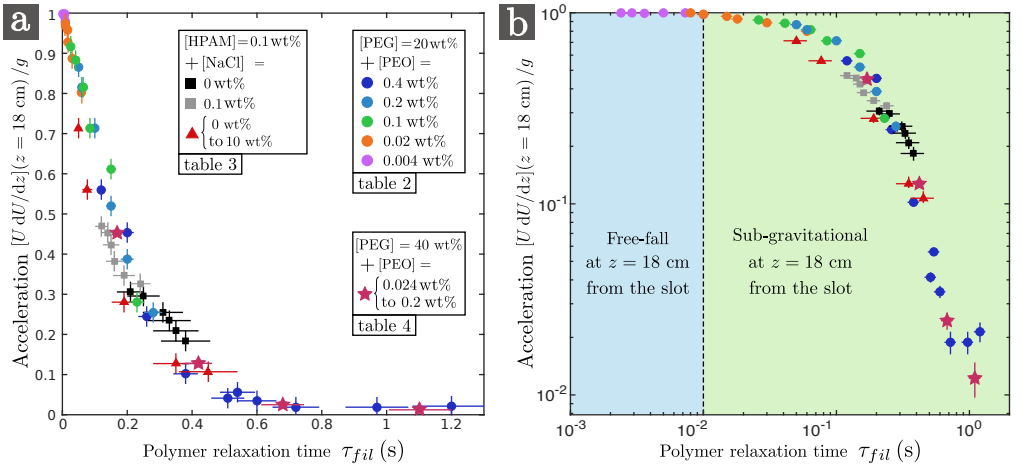

FIGURE 14. Dimensionless acceleration $[U\mathrm{d}U/\mathrm{d}z]/g$ at $z = 18$ cm from the slot against polymer extensional relaxation time τ_{fil} in lin-lin (a) and log-log (b) scales for all the solutions of tables 2 (PEO) and 3 (HPAM), for which the curtain length is always $L_c = 30$ cm, and for all PEO the solutions of tables 4 when the curtain length is also $L_c = 30$ cm. Note that another 0.4 wt% PEO solution with 20 wt% PEG solvent was prepared and that the curtain flow was measured at $t_d = 0$, 5, 10, and 20 minutes in order to fill the high relaxation time region of the curve.

points in the plot can correspond to very different values of the other rheological parameters. This result confirms that τ_{fil} plays a predominant role. The deviations can be explained by the differences in flow rates: curtains extruded at lower flow rates have a slightly lower acceleration, as discussed in §4.4. Note that some of the data presented in figure 14 correspond to the unstable

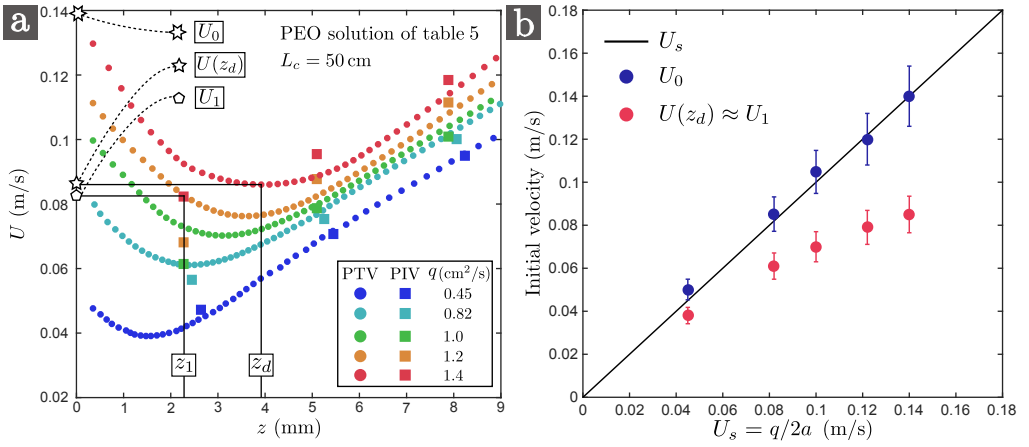

FIGURE 15. (a): Velocity field $U(z)$ at the slot exit measured from single particle tracking velocimetry (PTV) for the PEO solution of table 5 extruded at different flow rates q ranging between 0.45 cm^2/s and 1.4 cm^2/s. The curtain swells since the mean velocity decreases from U_0 at $z = 0$ to $U(z_d)$ at a distance z_d from the slot exit. U_0 is estimated by extrapolation the PTV data. The PIV velocity fields are also shown for comparison, the first value U_1 corresponding to $z_1 \approx 2.5$ mm. To guide the eye, z_1, z_d, U_0, U_1 and $U(z_d)$ are shown for the data corresponding to $q = 1.4$ cm^2/s. (b): The corresponding values of U_0 and $U(z_d)$ are plotted against the mean velocity $U_s = q/2a$ inside the slot.

curtains mentioned in §4.2. However, the instability does not seem to affect the average velocity field $U(z) = \langle\langle U\rangle_x\rangle_t$ since these data blend with the stable curtain data.

According to figure 14.b, solutions with relaxation times $\tau_{fil} \leqslant 10$ ms have an acceleration $U\mathrm{d}U/\mathrm{d}z = g$ at $z = 18$ cm from the slot exit. In fact, for some of these solutions, the local liquid acceleration is less than g close to the slot and reaches the free-fall value g at $z < 18$ cm. This is reminiscent of the flow of pure glycerin reported in figure 8, which suggests that g is also the asymptotic value of the liquid acceleration for viscoelastic curtains. However, due to the finite length of the curtain, many liquids are stopped before reaching the free-fall behaviour. This is particularly true for solutions with high relaxation times $\tau_{fil} \approx 1$ s which fall with very low accelerations $U\mathrm{d}U/\mathrm{d}z \approx 0.1$ m/s$^2 \ll g$ at $z = 18$ cm from the slot exit.

4.6. *Die swell*

We recall that the first value $U_1 = U(z_1)$ measured by PIV corresponds to the velocity at $z_1 \approx 2.5$ mm from the slot exit, whereas the mean velocity in the slot can be estimated as $U_s = q/2a$ where q is the measured linear flow rate and $2a$ is the slot thickness. Values of both U_s and U_1 are reported in tables 2, 3 and 4 for the corresponding curtains experiments. We observe that U_1 is systematically smaller than U_s, except for HPAM curtains, and that the ratio $\xi = U_s/U_1$ is up to 2 and increases with polymer concentration. Observations with the naked eye confirm that the curtain rapidly swells at the slot exit. This is not due to a wetting effect, as expected from the design of the die where the wall edges are bevelled (figure 1.b).

In order to estimate the velocity profile $U(z)$ in this region, we can use the particle tracking velocimetry (PTV) technique within the first millimetres of the flow, i.e. we track the position of singles particles after leaving the slot. Image processing is performed "manually". Results are presented in figure 15.a for the PEO solution of table 5 extruded at different flow rates. The liquid velocity first decreases from $U_0 = U(z = 0)$ at the slot exit to a minimum value at $z = z_d$ before finally increasing, where z_d ranges between 1.5 mm and 4 mm. PIV measurements are not able to capture this behaviour since cross-correlation is computed over centimetric windows. However, a superposition of the PIV velocity profiles in figure 15.a shows an acceptable agreement between

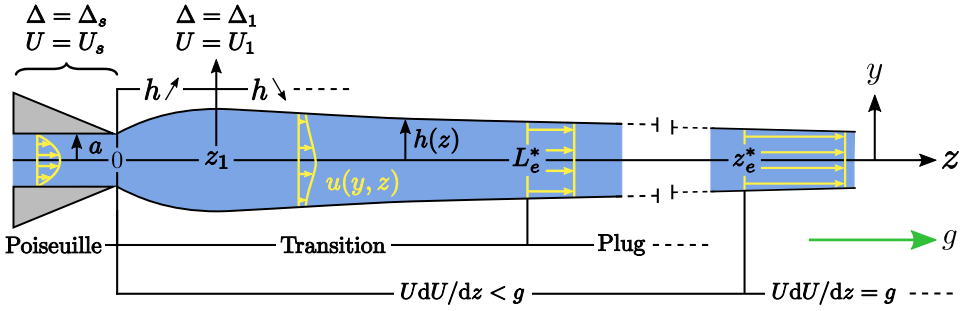

FIGURE 16. Sketch of an infinitely long viscoelastic curtain (cross-sectional view). During the swelling at the slot exit, the mean liquid velocity U and the mean normal stress difference $\Delta = \sigma_{zz} - \sigma_{yy}$ averaged over the curtain thickness switch respectively from U_s and Δ_s to U_1 and Δ_1 at $z_1 \approx 2.5$ mm from the slot exit. The local vertical velocity field $u(y,z)$ switches from a Poiseuille flow inside the slot to a plug flow at a distance $z = L_e^*$ from the slot. In parallel, the mean velocity field $U(z)$ is characterised by a transition from a sub-gravitational regime to an asymptotic free-fall regime at a distance $z = z_e^*$ from the slot.

the first value U_1 measured from PIV and the minimum velocity $U(z_d)$ measured from particle tracking: $U(z_d) = U_1$ with less than 15% error. The values of U_0 and $U(z_d)$ are reported in figure 15.b as a function of the mean velocity U_s in the slot. As expected, $U_0 = U_s$. Besides, the swelling ratio $\xi = U_s/U_1$ increases when increasing the flow rate. In the following, z_d and $U(z_d)$ are approximated by z_1 and U_1 for the sake of simplicity.

5. Theoretical description of the curtain flow

5.1. *General overview of the problem*

Before focusing on the theoretical description of the curtain flow, we would like to give in this section a general overview of the different types of flows involved in this problem. We first provide a qualitative description before focusing specifically on Newtonian liquids and viscoelastic liquids. The liquid first experiences a planar contraction of ratio A/a at the slot entrance (figure 1.b). The mean liquid velocity on the centre line $y = 0$ switches from about $q/2A$ in the hollow box to $U_s = q/2a$ inside the slot in a characteristic time a/U_s, where q is the linear flow rate and $2a$ is the slot thickness. Then, a Poiseuille flow is established in the slot due to the development of a viscous boundary layer along the walls. At the slot exit, the wall boundary condition switches to a free-surface boundary condition, i.e. zero shear stress at the liquid-air interface. Hence, due to viscous diffusion, the Poiseuille flow switches to a plug flow, as illustrated in figure 16. U is the mean vertical velocity averaged over the curtain thickness. After initial swelling at the slot exit, the curtain thickness decreases since fluid particles are now accelerated by gravity. Since the liquid may develop some resistance to gravitational forces, the local mean acceleration $U\mathrm{d}U/\mathrm{d}z$ may be initially less than g. The asymptotic free-fall regime where $U\mathrm{d}U/\mathrm{d}z = g$ is reached when inertia overcomes the resistance of the liquid.

For Newtonian liquids, a fully developed Poiseuille flow is expected to be established after a distance from the entrance of the slot which scales as $L_v = \rho U_s a^2/\eta = Re\, a$ with a prefactor typically less than one (Kays *et al.* 2005) where $Re = \rho U_s a/\eta$ is the Reynolds number. L_v is also the characteristic length scale of the transition from Poiseuille to plug. Hence, a large viscosity results in a fast transition. The plug flow is fully established at a distance $L_v^* = P_v L_v$ from the slot, where P_v is a dimensionless prefactor. In the case of axisymmetric laminar capillary jets, Sevilla (2011) shows that P_v is a function of the Weber number $We = \rho U_s^2 a/\gamma$ where a is the injector radius, and gives $P_v(We = 10) \approx 0.2$. Furthermore, the mean acceleration effectively reaches the asymptotic free-fall value g at a distance $z_v^* = F_v z_v$ ("v" for "viscous") from the slot where

$z_v = ((4\eta/\rho)^2/g)^{1/3}$ and where the prefactor F_v is a decreasing function of the initial curtain velocity (Brown 1961; Clarke 1968). In other words, $U\mathrm{d}U/\mathrm{d}z(z = z_v^*) \approx g$. A large viscosity results in a slow transition. Ignoring the prefactors, the ratio between the Poiseuille to plug and sub-gravitational to free-fall transition lengths is

$$\frac{L_v}{z_v} = Re\,\frac{a}{z_v} = \frac{U_s a^2 \rho^{5/3} g^{1/3}}{4^{2/3}\eta^{5/3}}, \tag{5.1}$$

which means that liquids of large viscosity ($L_v/z_v \ll 1$) exhibit a long sub-gravitational plug flow whereas liquids of low-viscosity ($L_v/z_v \gg 1$) fall with a mean acceleration g while exhibiting velocity gradients along the thickness direction.

We now focus on the viscoelastic liquids used in our experiments. For all solutions, the time scale a/U_s of the planar contraction is shorter than the extensional relaxation time τ_{fil}. Hence, the polymer molecules undergo a rapid strain of Hencky strain $\varepsilon \approx \ln(A/a) = 2.6$ (equation 3.7). Significant extensional stresses may arise due to this sudden polymer elongation. However, the time L_s/U_s spent by the liquid inside the slot is generally longer than τ_{fil}. Therefore, the polymeric stress developed by the liquid at the slot entrance is expected to relax towards the asymptotic Poiseuille flow value before leaving the slot. Moreover, since the Reynolds number ranges between 0.03 and 10 based on the zero-shear viscosity η_0, L_v ranges between 0.01 mm and 5 mm which is much smaller than the slot length $L_s = 10$ cm. This suggests that a fully developed Poiseuille flow is established long before the slot exit, as confirmed by direct visualisation.

Using analogous notations for Newtonian and viscoelastic curtains, let z_e^* ("e" for "elastic") be the distance from the slot at which the local acceleration of the liquid reaches the asymptotic value g. We showed in sections 4.1 and 4.5 that this transition length can be much larger than what could be expected from the theory of Newtonian curtains, i.e. $z_e^* \gg z_v^*$, and that it was mainly determined by the value of the extensional relaxation time τ_{fil} of the polymer solution. Of course, regardless of the liquid rheology, this discussion only makes sense if the curtain length is larger than this transition length, i.e. $L_c > z_e^*$ or $L_c > z_v^*$, otherwise the curtain flow would turn into a plane stagnation flow before reaching the free-fall regime.

Direct visualisation of the y dependence of the curtain flow is quite difficult. Therefore, to estimate the length L_e^* at which the plug flow is fully established in the case of viscoelastic liquids, we visualised the flow of some of PEO solutions when issuing from a nozzle of diameter 1 mm. For the degraded ($t_d = 100$ min) 0.1 wt% PEO solution with 20 wt% PEG solvent, we measure $L_e^* \approx 1.2$ cm although the transition to free-fall is out of frame in curtain experiments, i.e. $z_e^* > 18$ cm. Hence, provided that the order of magnitude of L_e^* is comparable in the curtain, we can reasonably assume that the plug flow is established much sooner than the free-fall regime, i.e. $L_e^*/z_e^* \ll 1$. We shall mention that our measurements suggest an influence of elasticity on the Poiseuille to plug transition: L_e^* is larger than what could be expected from the theory of Newtonian curtains. Further analysis is required to characterise this effect.

In this paper, we focus on the transition from the sub-gravitational regime to the free-fall regime. In particular, we wish to characterise the sub-gravitational regime in the case of a viscoelastic curtain and to express z_e^* as a function of the parameters of the problem.

5.2. *A master curve for Newtonian curtains*

As we will now show, the velocity field $U(z)$ of an infinitely long Newtonian curtain collapses on a master curve which, to the best of our knowledge, had not been clearly identified in the literature so far. This analytical description of Newtonian curtains will be a useful guide when describing the analogous case of viscoelastic curtains.

In 1961, Taylor proposed in the appendix of Brown (1961) the one-dimensional force balance equation 1.1 for the steady curtain flow of a Newtonian liquid of density ρ and dynamic

viscosity η. Surface tension is neglected and the gas surrounding the liquid is assumed to be dynamically passive. This equation is valid for slender curtain, i.e. $\mathrm{d}h/\mathrm{d}z \ll 1$ where $2h$ is the curtain thickness. Aidun (1987) and Ramos (1996) derived this equation rigorously from a long-wave approximation of the Navier-Stokes equation using the aspect ratio $a/L_c \ll 1$ as a small parameter, where $2a$ and L_c are respectively the slot thickness and the curtain length. Equation 1.1 can be put into non-dimensional form when rescaling by

$$\begin{cases} \bar{z} = z/z_v, \\ \bar{U} = U/U_v, \end{cases} \qquad z_v = \left(\frac{(4\eta/\rho)^2}{g}\right)^{1/3}, \qquad U_v = \sqrt{g\,z_v} = (4\eta g/\rho)^{1/3}, \tag{5.2}$$

We obtain

$$\bar{U}\bar{U}' = 1 + \bar{U}'' - \bar{U}'^2/\bar{U}, \tag{5.3}$$

where $'$ denotes spatial derivation $\mathrm{d}/\mathrm{d}\bar{z}$. The general solution of this equation was found by Clarke (1966, 1968) and is given by

$$\bar{U}(\bar{z}) = 2^{-1/3}\left[\left(\frac{\mathrm{Ai}'(Z) + C\,\mathrm{Bi}'(Z)}{\mathrm{Ai}(Z) + C\,\mathrm{Bi}(Z)}\right)^2 - Z\right]^{-1}, \qquad Z = 2^{-1/3}(\bar{z}+k), \tag{5.4}$$

where Ai and Bi are the Airy functions (Abramowitz & Stegun 1964) and C and k are integration constants that are to be determined from the upstream and downstream boundary conditions. Note that for a given value of C, varying k simply translates the curve along the $\bar{z}$-axis. This is due to the fact that $\bar{z}$ does not appear explicitly in equation 5.3.

The upstream boundary condition is simply

$$\bar{U}(\bar{z}=0) \equiv \bar{U}_0 = U_0/U_v = \rho U_0 z_v/4\eta, \tag{5.5}$$

where the initial liquid velocity U_0 at the slot exit can be chosen experimentally by varying the flow rate. Different types of downstream boundary conditions can be chosen depending on the particular experimental conditions (Ramos 1996). Imposing a large velocity at a given distance L_c from the slot corresponds to a film casting experiment where the liquid is collected by a drum rotating at constant angular velocity. This case corresponds to $C > 0$ in solution 5.4 (figure 17.a). On the other hand, the boundary condition $U(L_c) = 0$ leads to the transition to a plane stagnation flow where the liquid spreads onto a motionless horizontal solid plate placed at $z = L_c$ from the slot. In the latter case, which corresponds to $C < 0$ in solution 5.4 (figure 17.a), the liquid velocity first increases due to gravitational forces and reaches a maximum value at a distance z_m from the slot before finally decreasing down to 0 when approaching the stagnation point at $z = L_c$. According to figure 17.a, the presence of the solid plate only affects the flow within a distance from the plate which is of order $L_c - z_m$. In figure 17.b, we present $\bar{L}_c - \bar{z}_m = (L_c - z_m)/z_v$ against the dimensionless curtain length $\bar{L}_c = L_c/z_v$ for various initial velocities. These results suggest that $L_c - z_m$ is always less of equal to $2.3z_v$. However, as pointed out by Ramos (1996), the slender approximation is not justified near the stagnation point where the transverse velocity component becomes larger than the axial one. In this case, although solution 5.4 may be valid far enough from the impingement zone, a two-dimensional analysis is required when focusing on this zone. We can however reasonably assume that the presence of the solid plate only affects the flow within a distance before impact which is of order z_v.

According to the previous results, if the curtains length is $L_c \gg z_v$, the flow close to the slot is universal and is not influenced by the downstream boundary condition. Therefore, in order to characterise this universal flow far from the impingement zone, we can use the following boundary condition

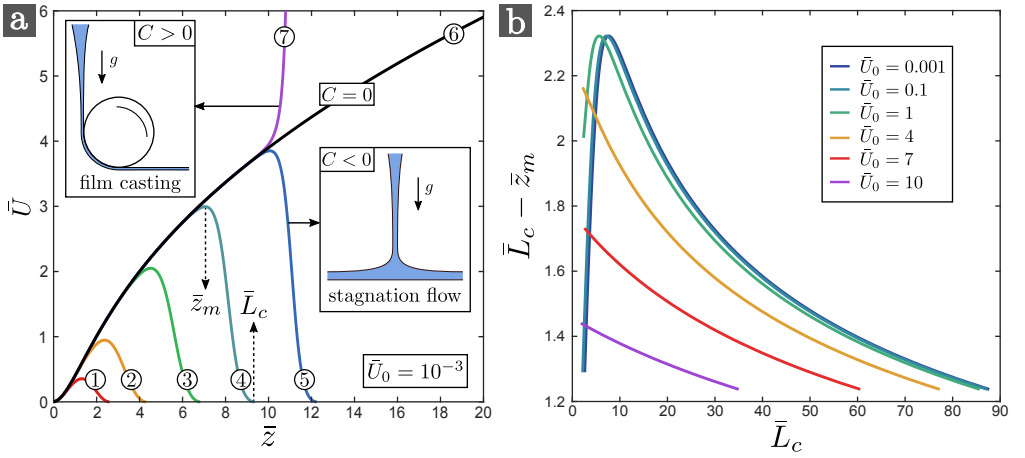

FIGURE 17. (a): Clarke's solution (equation 5.4) for $C = -10^2$ (1), $C = -10^{-1}$ (2), $C = -10^{-3.5}$ (3), $C = -10^{-7}$ (4), $C = -10^{-12}$ (5), $C = 0$ (6) and $C = +10^{-12}$ (7), where k is chosen to ensure that the initial velocity is $\bar{U}_0 = 10^{-3}$ for each curve. Solutions with $C < 0$, $C = 0$ and $C > 0$ correspond to different types of downstream boundary condition, respectively a plane stagnation flow for $C < 0$ where $U(\bar{L}_c) = 0$ when impacting a flat solid plate at a distance $L_c = \bar{L}_c z_v$ from the slot, an infinite curtain which converges to a free-fall for $C = 0$, and a film casting experiment for $C > 0$ where the velocity imposed by the rotation speed of the drum can be arbitrarily large. When $C < 0$, the presence of the solid plate only affects the flow within a (dimensionless) distance from the plate which is of order $\bar{L}_c - \bar{z}_m$ where $\mathrm{d}U/\mathrm{d}\bar{z}(\bar{z} = \bar{z}_m) = 0$. (b): $\bar{L}_c - \bar{z}_m$ against $\bar{L}_c$ for different initial velocities $\bar{U}_0$. Since varying k for a given C only translates the curve along the $\bar{z}$-axis in equation 5.4, $\bar{L}_c - \bar{z}_m$ does not depend on k. Hence, all the curves in (b) corresponding to different values of $\bar{U}_0$ can be deduced from each other by simple translation along the $\bar{L}_c$-axis.

$$\lim_{\bar{z}\to\infty} \bar{U}\bar{U}' = 1, \tag{5.6}$$

which ensures that the flow would converge asymptotically to a free-fall with constant acceleration g for a curtain of infinite length. This boundary condition corresponds to $C = 0$ in solution 5.4 (figure 17.a). It is the case discussed by Clarke (1966, 1968). In curtain coating, note that the liquid falls onto a horizontal solid surface moving horizontally at constant speed, which breaks the symmetry of the problem. However, we can reasonably assume that the flow far from the impingement zone is also not influenced by this boundary condition.

Analytical solutions $\bar{U}(\bar{z})$ are shown in figure 18.a for $C = 0$ and initial velocities $\bar{U}_0$ ranging between 0 and 2. The curves are similar. In fact, they all rescale on a unique master curve after translation along the $\bar{z}$ axis. Indeed, let M_v ("M" for "Master curve") be the particular solution corresponding to $\bar{U}_0 = 0$. We have

$$M_v(\bar{z}) = 2^{-1/3}\left[\left(\frac{\mathrm{Ai}'(Z)}{\mathrm{Ai}(Z)}\right)^2 - Z\right]^{-1}, \qquad Z = 2^{-1/3}(\bar{z} + k_0), \tag{5.7}$$

where $\mathrm{Ai}(2^{-1/3}k_0) = 0$ which gives $k_0 \approx -2.94583$. Of course, achieving a curtain of zero initial velocity with infinite initial thickness is not physically possible. Yet, we can easily demonstrate that any physical solution with initial velocity $\bar{U}_0 > 0$ writes

$$\bar{U}(\bar{z}) = M_v\left(\bar{z} + M_v^{-1}(\bar{U}_0)\right), \tag{5.8}$$

where M_v^{-1} is the functional inverse of M_v. Hence, any solution $\bar{U}(\bar{z})$ with initial velocity $\bar{U}_0 > 0$ will collapse on the master curve $M_v(\bar{z})$ after translation along the $\bar{z}$ axis by a distance $M_v^{-1}(\bar{U}_0)$

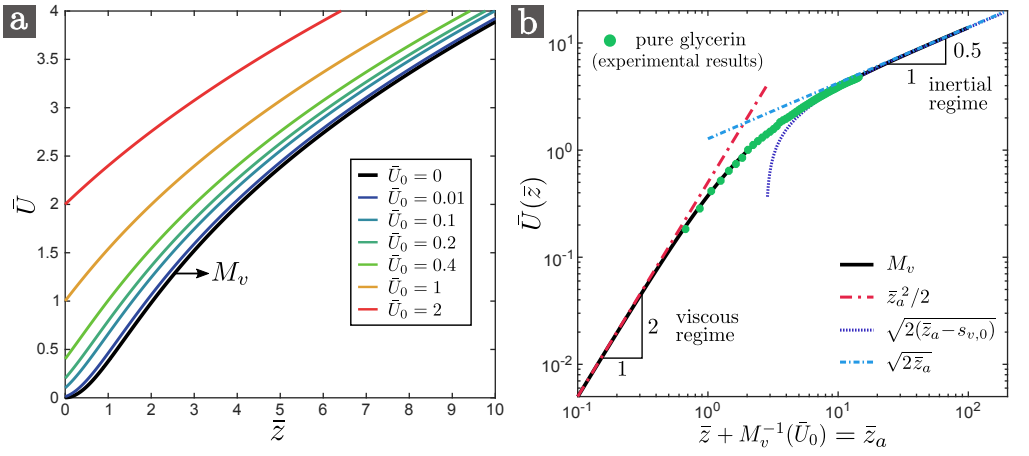

FIGURE 18. (a): Dimensionless velocity field $\bar{U}(\bar{z})$ for an infinitely long curtain made of a Newtonian liquid (equation 5.4 for $C = 0$), starting from various initial velocities $\bar{U}_0$ ranging between 0 and 2. All the curves for $\bar{U}_0 > 0$ collapse on the master curve M_v corresponding to $\bar{U}_0 = 0$ after translation of each curve along the $\bar{z}$ axis by a distance $M_v^{-1}(\bar{U}_0)$ (equation 5.8). (b): Confirmation with the experimental velocity field of the pure glycerin curtain of figure 8 where $\bar{U}_0 = 0.14$. The master curve M_v is characterised by an initial sub-gravitational viscous regime and an asymptotic free-fall regime (equation 5.9).

on the right. For the glycerin curtain in figure 8, we have $\bar{U}_0 = 0.14$ and $M_v^{-1}(\bar{U}_0) = 0.55$. Therefore, shifting the dimensionless profile $\bar{U}(\bar{z})$ by a distance 0.55 on the right makes the experimental data collapse on the master curve, as shown in figure 18.b.

The master curve is characterised by two regimes:

$$M_v(\bar{z}) = \begin{cases} \bar{z}^2/2 & \bar{z} \ll 1 : \text{viscous regime,} \\ \sqrt{2\,(\bar{z} - s_{v,0})} & \bar{z} \gg 1 : \text{inertial regime,} \end{cases} \tag{5.9}$$

where $s_{v,0} \approx 2.8$. The initial viscous regime ($\bar{z} \ll 1$) corresponds to a balance between gravity and viscous forces where inertia is negligible in equation 1.1. As the liquid velocity increases, we enter into an intermediate inertio-viscous regime where none of the terms of equation 1.1 can be neglected. Finally, inertia dominates over viscous forces for $\bar{z} \gg 1$ and the local acceleration reaches the asymptotic free-fall value.

For real curtains with non-zero initial velocity U_0, according to equations 5.8 and 5.9, the viscous regime only exists if U_0 is much smaller than U_v, i.e. $\bar{U}_0 \ll 1$. This is illustrated in figures 19.a and 19.b where we plot the local extension rate $\bar{U}'(\bar{z})$ and the local acceleration $\bar{U}\bar{U}'(\bar{z})$ for $C = 0$ and initial velocities $\bar{U}_0$ ranging between 0 and 10. For low values of $\bar{U}_0$, $\bar{U}'$ first increases (viscous regime) before finally decreasing (inertial regime). However, as $\bar{U}_0$ increases, $\bar{U}'$ becomes a monotonous decreasing function. Equivalently, the acceleration at the slot exit $\bar{U}\bar{U}'(0)$ goes from 0 for $\bar{U}_0 = 0$ to 1 for $\bar{U}_0 \gg 1$, i.e. inertia dominates over viscous forces even close to the slot. In practice, we can assume that the flow of a Newtonian curtain is very well approximated by a free-fall $\bar{U}^2 = \bar{U}_0^2 + 2\bar{z}$ if $\bar{U}_0 \geqslant 10$. Physically, it can be explained by considering $\bar{U}_0$ as a Reynolds number based on the characteristic length z_v (equation 5.5).

In the case of a negligible initial velocity $U_0 \ll U_v$, according to equations 5.8 and 5.9, the viscous regime of the flow ($z \ll z_v$) writes

$$\bar{U}(\bar{z}) = \frac{1}{2}\left(\bar{z} + \sqrt{2\bar{U}_0}\right)^2. \tag{5.10}$$

This regime has not received much attention in the literature since achieve such a flow experimen-

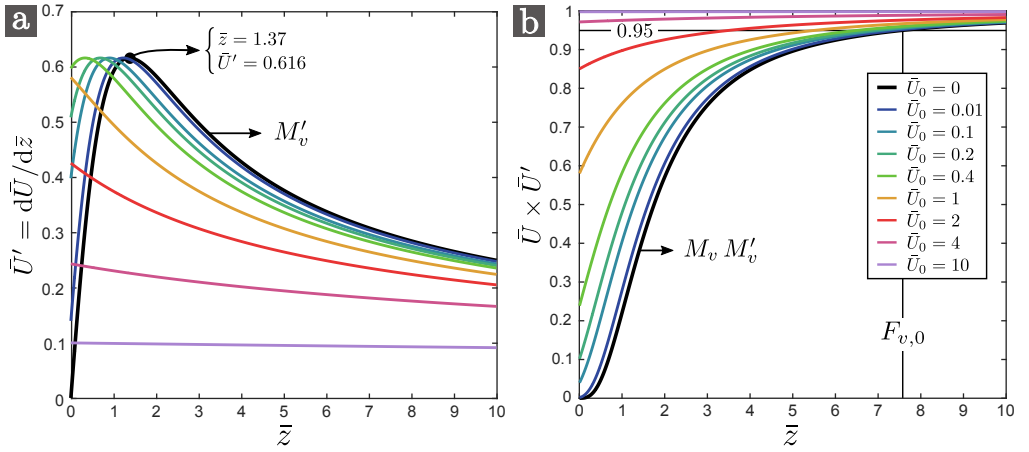

FIGURE 19. Dimensionless extension rate $\bar{U}'(\bar{z})$ (a) and acceleration $\bar{U}\bar{U}'(\bar{z})$ (b) for an infinitely long curtain made of a Newtonian liquid (equation 5.4 for $C = 0$), starting from various initial velocities $\bar{U}_0$ ranging between 0 and 10. The master curve M_v has an inflection point at $\bar{z} \approx 1.37$, where the elongation rate reaches a maximum value $M'_v(1.37) \approx 0.616$, and reaches the asymptotic free-fall regime at $\bar{z} = F_{v,0} \approx 7.56$ since $M_v M'_v(F_{v,0}) = 0.95$, where 0.95 is an arbitrary value close to 1.

tally is quite difficult. Indeed, z_v has to be of the order of a few centimetres, which implies using a liquid of dynamic viscosity $\eta \geqslant 10^1$ Pa.s. Besides, in addition to the difficulty of achieving a large enough flow rate to maintain a continuous curtain, one must use a die of large width l in order to avoid the edge effects due to the presence of the vertical guides (§2.4). Finally, the curtain length L_c has to be larger than z_v to observe the universal behaviour which is not affected by the downstream boundary condition.

Regardless of the value of the initial velocity, in the inertial regime, again using equations 5.8 and 5.9, the dimensionless velocity field writes

$$\bar{U}(\bar{z}) = \sqrt{\bar{U}_0^2 + 2(\bar{z} - s_v)}, \tag{5.11}$$

where $s_v = s_{v,0} + \bar{U}_0^2/2 - M_v^{-1}(\bar{U}_0)$. In his early experiments, Brown (1961) found $s_v = 2$. For negligible initial velocities $U_0 \ll U_v$, this regime is observed for $z \gg z_v$. For large initial velocities $U_0 \gg U_v$, it is observed immediately after the slot exit. In fact, since s_v goes to 0 for $U_0 \gg U_v$, we recover the free-fall $U^2 = U_0^2 + 2gz$.

We can now derive an expression of the length z_v^* of the sub-gravitational part of the curtain introduced in §5.1. Let us define this length as $U\mathrm{d}U/\mathrm{d}z(z = z_v^*) = 0.95g$ where 0.95 is an arbitrary value close to 1. For $\bar{U}_0 = 0$, let $F_{v,0}$ be such that $M_v M'_v(\bar{z} = F_{v,0}) = 0.95$. We obtain $F_{v,0} \approx 7.56$ (figure 19.b). Therefore, according to equation 5.8, we have

$$z_v^* = F_v z_v, \qquad F_v = F_{v,0} - M_v^{-1}(\bar{U}_0), \tag{5.12}$$

where the prefactor F_v is a decreasing function of the initial velocity. This result holds if $F_v \geqslant 0$, i.e. if $\bar{U}_0 \leqslant M_v(F_{v,0}) \approx 3.23$. For numerical applications, note that $F_v \approx 2.34\,(3.23 - \bar{U}_0)$ with an error less than 0.65. This result had not been derived in the literature so far since the master curve had not been explicitly identified.

5.3. *General force balance equation*

As will be presented in §5.4, many aspects of the Newtonian curtains theory presented in the previous section are analogous to the description of viscoelastic curtains. Hence, in order to

find the appropriate length and velocity scales of viscoelastic curtains, let us first generalise the Newtonian force balance equation 1.1 to any continuous material.

A slice of curtain between altitudes z and $z+\mathrm{d}z$ travels a distance $\mathrm{d}z = U\mathrm{d}t$ between times t and $t+\mathrm{d}t$. Its momentum per unit curtain width is $2h\rho U\mathrm{d}z$. We consider the gravitational force $2h\rho g\mathrm{d}z$ and the contact forces $2h(z)\pi_{zz}(z)$ and $2h(z+\mathrm{d}z)\pi_{zz}(z+\mathrm{d}z)$ acting respectively on the upper and lower side, where π is the mean stress tensor. Using the flow rate conservation

$$2hU = q = 2aU_s, \tag{5.13}$$

along with $\mathrm{d}z = U\mathrm{d}t$, we obtain

$$U\frac{\mathrm{d}U}{\mathrm{d}z} = g + \frac{U}{\rho q}\frac{\mathrm{d}(2h\pi_{zz})}{\mathrm{d}z}. \tag{5.14}$$

This equation can be derived rigorously from a long-wave approximation of the Cauchy equation and is valid for slender curtain, i.e. $\mathrm{d}h/\mathrm{d}z \ll 1$. Note that the mean quantities can be written as

$$U = \frac{1}{h}\int_0^h u\,\mathrm{d}y \qquad \text{and} \qquad \pi_{zz} = \frac{1}{h}\int_0^h \pi^*_{zz}\mathrm{d}y, \tag{5.15}$$

where $u(y,z)$ and $\pi^*_{zz}(y,z)$ are respectively the vertical component of the local velocity field and the normal component of the local stress tensor π^*. Let us write $\pi^*_{ij} = -P^*\delta_{ij} + \sigma^*_{ij}$ for the local tensor and $\pi_{ij} = -P\delta_{ij} + \sigma_{ij}$ for the mean tensor. For example, in the Newtonian case, we have $\sigma^*_{zz} = 2\eta\,\partial u/\partial z$ and $\sigma^*_{yy} = 2\eta\,\partial v/\partial y$ where v is the transverse component of the local velocity field, which gives $\sigma_{zz} = 2\eta\,\mathrm{d}U/\mathrm{d}z$ and $\sigma_{yy} = -2\eta\,\mathrm{d}U/\mathrm{d}z$ for an incompressible flow. Neglecting surface tension and using the slender curtain approximation, we can assume that $\pi_{yy} = -P_a$ where P_a is the atmospheric pressure (Brown 1961). This leads to $P(z) = P_a + \sigma_{yy}$ and therefore $\pi_{zz} = -P_a + (\sigma_{zz} - \sigma_{yy})$. Normalising pressure such that $P_a = 0$, and defining the mean normal stress difference $\Delta \equiv \sigma_{zz} - \sigma_{yy}$, we can finally write the general force balance equation

$$U\frac{\mathrm{d}U}{\mathrm{d}z} = g + \frac{U}{\rho}\frac{\mathrm{d}}{\mathrm{d}z}\left(\frac{\Delta}{U}\right). \tag{5.16}$$

This equation is valid for any continuous material. In the case of a Newtonian liquid, we have $\Delta = 4\eta\mathrm{d}U/\mathrm{d}z$ and we recover equation 1.1. In the case of a viscoelastic liquid, a more general constitutive equation must be used to close the system. Note that equation 5.16 can reasonably be used for the curtains presented in this paper since the local slenderness ratio $|\mathrm{d}h/\mathrm{d}z|$ is less than one. The data of figure 15 are a typical example where $\mathrm{d}h/\mathrm{d}z$ goes from $+0.1$ at $z=0$ to a minimum value of about -0.06 after die swell, and is of order -10^{-4} at $z = 20$ cm from the slot.

We can use equation 5.16 to find the appropriate scalings of viscoelastic curtain flows without specifying any particular form of the constitutive equation. We know from the experimental results of §4.5, that the extensional relaxation time τ_{fil} of the solution is of primary importance. Therefore, let us write equation 5.16 in a Lagrangian form where we introduce time

$$t = \int_0^z \mathrm{d}z^*/U(z^*). \tag{5.17}$$

We obtain

$$\frac{\mathrm{d}U}{\mathrm{d}t} = g + \frac{1}{\rho}\frac{\mathrm{d}}{\mathrm{d}t}\left(\frac{\Delta}{U}\right), \tag{5.18}$$

which can be integrated into

$$U - U_1 = g(t - t_1) + \frac{1}{\rho}\left(\frac{\Delta}{U} - \frac{\Delta_1}{U_1}\right), \tag{5.19}$$

where subscript $_1$ refers to any altitude z_1. Introducing τ_{fil} which is the natural time scale of the polymers, we obtain the dimensionless force balance equation

$$\frac{U - U_1}{g\tau_{fil}} = \frac{t - t_1}{\tau_{fil}} + \frac{\Delta}{\rho g U \tau_{fil}} - \frac{\Delta_1}{\rho g U_1 \tau_{fil}}. \tag{5.20}$$

This equation suggests that the natural velocity scale of the flow is

$$U_e = g\tau_{fil}. \tag{5.21}$$

Therefore, the natural length scale of the flow is $z_e = U_e\,\tau_{fil}$ which gives

$$z_e = g\tau_{fil}^2 = U_e^2/g. \tag{5.22}$$

5.4. *A master curve for viscoelastic curtains*

By analogy with Newtonian curtains, we can now use the scalings 5.21 and 5.22 to identify the master curve of the viscoelastic curtain flow. First, we plot $U(z)/U_e$ as a function of $(z - z_1)/z_e$ where $z_1 \approx 2.5$ mm (not shown). We obtain similar curves which, like in figure 18.a, seem to rescale on a unique master curve after translation along the horizontal axis. Indeed, when shifting each curve by a certain dimensionless distance z_{shift}, we obtain a good collapse of the velocity profiles with less than 20% error, as shown in figure 20.a in log-log scale. Our experimental data covers seven decades in z/z_e. We introduce dimensionless variables

$$\hat{z} = z/z_e\,, \qquad \hat{U} = U/U_e. \tag{5.23}$$

The master curve $M_e(\hat{z})$ is characterised by two regimes:

$$M_e(\hat{z}) = \begin{cases} K\hat{z}^{\alpha} & \hat{z} \ll 1 : \text{elastic regime,} \\ \sqrt{2\,(\hat{z} - s_{e,0})} & \hat{z} \gg 1 : \text{inertial regime,} \end{cases} \tag{5.24}$$

where $K = 1.3 \pm 0.2$ and $\alpha = 0.92 \pm 0.02$. Note that we only consider in figure 20.a the experimental data which are presumably not influenced by the downstream boundary condition. This includes the unstable HPAM curtains mentioned in §4.2, showing that the instability does not affect the average velocity field. This result also confirms that the shear rheology parameters such as η_0 and n are irrelevant in the description of the curtain flow, as well as the flexibility parameter b. We measure that M_e^2 reaches an oblique asymptote of equation $M_e^2 = 2(\hat{z} - s_{e,0})$ in the free-fall regime where $s_{e,0} = 7 \pm 2$.

The value of z_{shift}, which is specific to each velocity field, is presented in figure 20.b as a function of the dimensionless initial velocity $\hat{U}_1 = U_1/U_e$ where $U_1 = U(z_1)$. We measure that $z_{shift} \approx (\hat{U}_1/K)^{1/\alpha}$ for low initial velocities $\hat{U}_1 \ll 1$ and that $z_{shift} \approx \hat{U}_1^2/2$ for large initial velocities $\hat{U}_1 \gg 1$, which suggests that $z_{shift} = M_e^{-1}(\hat{U}_1)$. Finally, we can write that

$$\hat{U}(\hat{z}) = M_e\left(\hat{z} - \hat{z}_1 + M_e^{-1}(\hat{U}_1)\right), \tag{5.25}$$

which is completely analogous to the Newtonian curtain flow since equation 5.8 also gives $\bar{U}(\bar{z}) = M_v\left(\bar{z} - \bar{z}_1 + M_v^{-1}(\bar{U}_1)\right)$ for any altitude $z_1 \geqslant 0$. However, since the die swell flow for $0 < z < z_1$ is not captured by equation 5.24, equation 5.25 is only valid for $z \geqslant z_1$. In particular, $\hat{U}(\hat{z}) \neq M_e\left(\hat{z} + M_e^{-1}(\hat{U}_0)\right)$ where $\hat{U}_0 = U_0/U_e$.

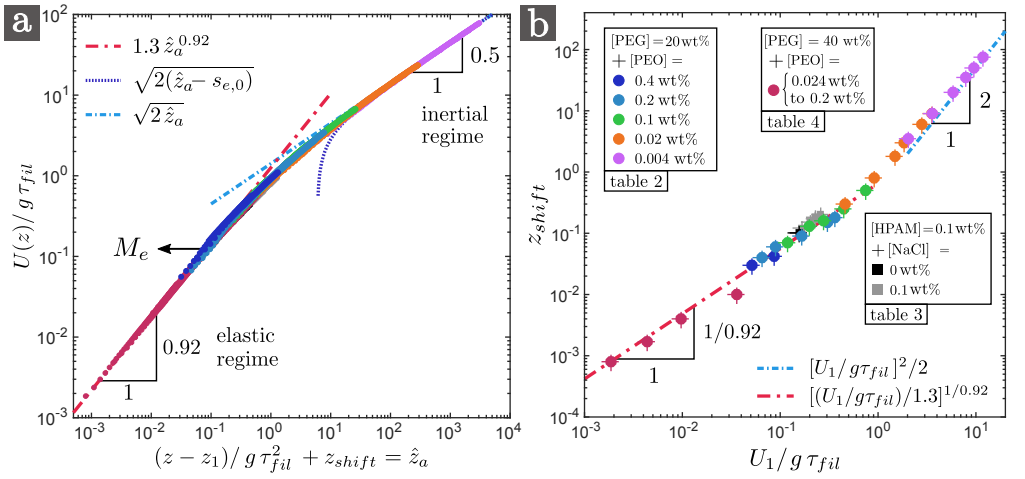

FIGURE 20. (a): Master curve of viscoelastic curtains. Dimensionless velocity field $U(z)/g\tau_{fil}$ against $(z-z_1)/g\tau_{fil}^2+z_{shift}$ in log-log scale, where $z_1 \approx 2.5$ mm, and where each curve is translated by a distance z_{shift} in order to rescale all the data on a single curve. The master curve M_e is characterised by an initial sub-gravitational elastic regime and an asymptotic free-fall regime (equation 5.24). (b): When plotting z_{shift} against $U_1/g\tau_{fil}$, we find that $z_{shift} = M_e^{-1}(U_1/g\tau_{fil})$. We only consider the curtain flows which are presumably not influenced by the downstream boundary condition. For the PEO solutions with 40 wt% PEG solvent of table 4, we only take the longest curtains, for example $L_c = 200$ cm for the data of figure 11.a. Besides, for the PEO and HPAM solutions of tables 2 and 3 (top) which correspond to curtains of length $L_c = 30$ cm, we show the velocity profile for $z < 20$ cm only for the solutions with extensional relaxation times $\tau_{fil} \leqslant 0.2$ s since the experiments reported in §4.3 suggest that the effect of the downstream boundary condition is out of frame.

According to equations 5.25 and 5.24, the elastic regime only exists if U_1 is much smaller than U_e, i.e. $\hat{U}_1 \ll 1$. If $\hat{U}_1 \ll 1$, according to these equations, the elastic regime of the flow ($z \ll z_e$) writes

$$\hat{U}(\hat{z}) = K\left(\hat{z} - \hat{z}_1 + (\hat{U}_1/K)^{1/\alpha}\right)^{\alpha}, \tag{5.26}$$

and corresponds to negligible inertia in the force balance equation 5.16. Note that only two curtains exhibit such a fully developed elastic regime: the 0.2 and 0.11 wt% PEO solutions with 40 wt% PEG solvent (table 4). For these solutions, the curtain flow is the same within the first 30 cm of the fall for both $L_c = 1.5$ m and 2 m which suggests that the flow has become independent of the downstream boundary condition (figure 11.a). However, $z_e = g\tau_{fil}^2$ is respectively $z_e = 12$ m and $z_e = 4.5$ m. Hence, we are not in the ideal limit $L_c \gg z_e$. Therefore, it is not excluded that the data corresponding to the elastic regime in figure 20.a are still a bit sensitive to the downstream boundary condition. If that is the case, a curtain of length $L_c \gg z_e$ would potentially exhibit an elastic regime with a value of α closer to 1. Of course, achieving such curtains is very difficult since they would probably break before reaching the free-fall regime due to the shear instability mentioned in §4.3.

Note that the transition to plane stagnation flow discussed in §4.3 for viscoelastic curtains is analogous to the Newtonian case. In both figures 11 and 17, the liquid velocity first increases, reaches a maximum value at some distance z_m from the slot, and finally decreases down to $U(L_c) = 0$. Provided that the analogy remains true, we speculate that the presence of the plate affects the viscoelastic curtain flow within a distance from the plate which is of order z_e.

Regardless of the value of the initial velocity, in the inertial regime, again using equations 5.25 and 5.24, the dimensionless velocity field writes

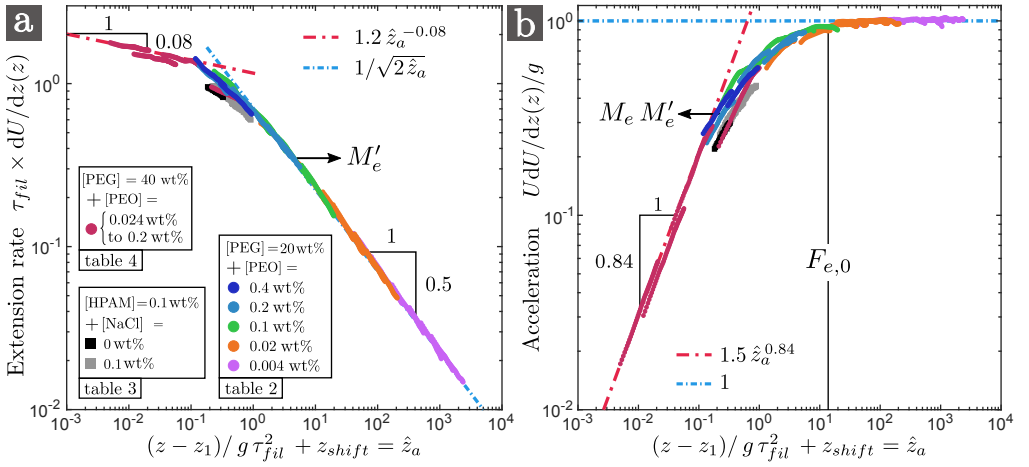

FIGURE 21. (a) Dimensionless extension rate $\tau_{fil}\,dU/dz(z)$ and (b) dimensionless acceleration $U dU/dz(z)/g$ versus $(z-z_1)/z_e + z_{shift}$ for the curtains of figure 20. The master curve M_e reaches the asymptotic free-fall regime at z/z_e about $F_{e,0} = 12 \pm 5$ since $M_e\, M_e'(F_{e,0}) = 0.95$, where 0.95 is an arbitrary value close to 1.

$$\hat{U}(\hat{z}) = \sqrt{\hat{U}_1^2 + 2(\hat{z} - \hat{z}_1 - s_e)}, \tag{5.27}$$

where $s_e = s_{e,0} + \hat{U}_1^2/2 - M_e^{-1}(\hat{U}_1)$. In the case of a negligible initial velocity $U_1 \ll U_e$, this regime is reached for $z \gg z_e$. On the other hand, for initial velocities $U_1 \gg U_e$, inertia dominates over viscous forces even close to the slot and the flow is well approximated by a free-fall $U^2 = U_1^2 + 2g(z - z_1)$ since s_e goes to zero.

In figure 21.a and 21.b, we present respectively the dimensionless extension rate $\dot{\varepsilon}\tau_{fil}$ where $\dot{\varepsilon} = dU/dz$ and the dimensionless acceleration $[U dU/dz]/g$ as a function of $\hat{z} - \hat{z}_1 + z_{shift}$. The experimental data collapse on master curves which correspond to M_e' and $M_e M_e'$ respectively, where $'$ denotes spatial derivation $d/d\hat{z}$. According to figure 21.a, the extension rate is of the order of $1/\tau_{fil}$ in the elastic regime $z \ll z_e$. More precisely, $\dot{\varepsilon}\tau_{fil}$ weakly decreases and is initially larger than the coil-stretch transition value $1/2$. This result is reminiscent of the filament thinning experiment described in §3.2 for which $\dot{\varepsilon}\tau_{fil} = 2/3$ in the elastic regime.

We can now derive an expression of the length z_e^* of the sub-gravitational part of the curtain introduced in §5.1. Let us define this length as $U dU/dz(z = z_e^*) = 0.95g$ where 0.95 is an arbitrary value close to 1 and let $F_{e,0}$ be such that $M_e M_e'(\hat{z} = F_{e,0}) = 0.95$. We obtain $F_{e,0} = 12 \pm 5$ (figure 21.b). Therefore, according to equation 5.25, we have

$$z_e^* = F_e\, z_e, \qquad F_e = F_{e,0} + \hat{z}_1 - M_e^{-1}(\hat{U}_1), \tag{5.28}$$

where the prefactor F_e is a decreasing function of the initial velocity.

5.5. *Inelastic viscous curtains versus low-viscosity elastic curtains*

In the previous sections, we have characterised the curtain flow of both Newtonian and viscoelastic liquids. In particular, the length of the sub-gravitational part of the curtain is given respectively by z_v and z_e (equations 5.2 and 5.22) with prefactors which are decreasing functions of the initial velocity. For a given viscoelastic liquid with zero-shear viscosity η_0, density ρ and extensional relaxation time τ_{fil}, we define a Weissenberg number

$$Wi = \left(\frac{z_e}{z_v}\right)^{1/2} = \frac{\tau_{fil}\, g^{2/3}}{(4\eta_0/\rho)^{1/3}}, \tag{5.29}$$

which measures the relative importance of elastic to viscous effects in the curtain flow. Values of Wi are reported in tables 2, 3 and 4. As expected, it is larger than one since $z_e \gg z_v$ in our experiments, except for solutions with low polymer concentrations exhibiting a free-fall, for which both z_e and z_v are less than a few millimetres. When adding polymer molecules to a viscous Newtonian solvent with a large value of z_v, we can expect a transition from the viscous regime described in §5.2 with exponent 2 (equation 5.10) to the elastic regime described in §5.4 with exponent $\alpha = 0.92$ (equation 5.26) when Wi becomes larger than one.

6. Elastic stress at the slot exit

In this section, we address the question of the origin of the elastic stress in the curtain. One possible origin might be some unrelaxed fraction of the polymeric stress developed in the slot. To test this, we first investigate the die swell ratio.

6.1. *The die swell ratio*

The liquid swells at the slot exit due to the recovery of the elastic strain imparted into the die. In the theory of Tanner (1970, 2005), and Huang & White (1979), the swelling ratio is

$$\xi = \frac{U_s}{U_1} = \left[1 + \frac{3-m}{m+1}\left(\frac{N_1}{2\sigma}\right)^2_w\right]^{1/4}, \tag{6.1}$$

where $N_1 = \sigma^*_{zz} - \sigma^*_{yy}$ and $\sigma = \sigma^*_{yz}$ are respectively the normal stress difference and the shear stress, m is such that $N_1 \propto \sigma^m$, and subscript $_w$ indicates that N_1 and σ are to be taken at the wall of the slot, i.e. at $y = a$. Note that σ^* is the local stress tensor. Let us compare the experimental data presented in figure 15 for the PEO solution of table 5 with Tanner's prediction 6.1. The wall shear stress $\dot{\gamma}_w$ is of order U_s/a which is larger than the shear rate $\dot{\gamma}_c = 3\ \mathrm{s}^{-1}$ at which shear-thinning starts. Hence, the Carreau law 3.1 can be reduced to an Ostwald power law $\sigma = K_0\dot{\gamma}^n$ with $K_0 = \eta_0/\dot{\gamma}_c^{n-1}$. For shear-thinning fluids following an Ostwald power, the wall shear rate in a planar Poiseuille flow is

$$\dot{\gamma}_w = \frac{2n+1}{n}\,\frac{U_s}{a}. \tag{6.2}$$

With U_s ranging between 0.045 and 0.14 m/s and $n = 0.81$, we find that $\dot{\gamma}_w$ ranges between 290 and 900 s^{-1}. We can reasonably use the parameters of table 5 since shear rheology measurements are performed for shear rates up to 700 s^{-1} which is of the order of $\dot{\gamma}_w$.

The experimental die swell ratio ξ is shown in figure 22 along with the values predicted by equations 6.1 and 6.2. The theory clearly overpredicts the die swell ratio. Indeed, the unconstrained recovery theory of Tanner is only valid if the extruded sheet is load-free, i.e. in the absence of gravity, where the curtain reaches a constant thickness and falls with constant mean velocity after swelling. According to the force balance equation 5.16, the mean normal stress difference in the curtain must be constant. In the theory of Tanner, it is assumed that most fluid particles "rapidly" switch from the state of fully developed flow in the slot to a state of zero stress measured relative to atmospheric pressure as datum. Here, "rapidly" means that the time needed to clear the exit zone is short compared to the polymer relaxation time, i.e. $U_s\tau_{fil}/a \gg 1$ which is the case in figure 22. In other words, the mean normal stress difference Δ defined in §5.3 by

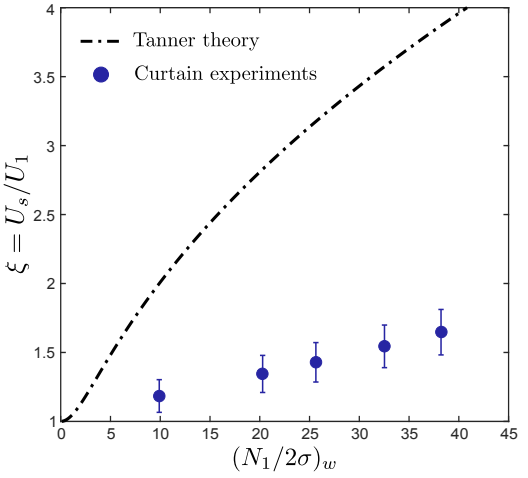

FIGURE 22. Comparison between the experimental die swell ratio $\xi = U_s/U_1$ for the data of figure 15 and the values predicted by Tanner's unconstrained recovery theory (equation 6.1) where we use $(N_1)_w = N_1(\dot{\gamma}_w) = \Psi\dot{\gamma}_w^{\alpha_1}$ and $(\sigma)_w = \sigma(\dot{\gamma}_w) = K_0\dot{\gamma}_w^n$ where $\dot{\gamma}_w$ is the wall shear rate (equation 6.2). Since $N_1 \propto \sigma^m$, we use $m = \alpha_1/n$.

$$\Delta = \frac{1}{h}\int_0^h (\sigma_{zz}^* - \sigma_{yy}^*)\,\mathrm{d}y, \tag{6.3}$$

switches from a value Δ_s inside the slot to a value Δ_1 after swelling which is $\Delta_1 = 0$ in the absence of gravity. The discrepancy in figure 22 suggests that $\Delta_1 \neq 0$ in the presence of an axial tension due to gravity, where $\Delta_1 = \Delta(z_1)$ (figure 16).

In the presence of gravity, the die swell ratio is generally assumed to be only slightly modified in the case of jets extruded from a hole (Richardson 1970). However, in the planar case, Huang & White (1979) report significant discrepancies between Tanner's theory and their experimental results when extruding polystyrene melts from slit dies into ambient air, like in figure 22. They report that Tanner's law was recovered when extruding into a bath of silicone oil with the same density, in which case the curtain no longer necks down after swelling due to gravity.

These results suggest that the elastic stress imparted into the die may have an effect on the curtain flow downstream. In order to quantify this effect, let us compare the value of the mean normal stress difference Δ_s inside the die and Δ_1 after swelling.

6.2. *Mean normal stress difference before and after swelling*

Δ_s can be estimated analytically. We consider a shear-thinning fluid following an Ostwald power law $\sigma = K_0\dot{\gamma}^n$ for simplicity. Assuming a fully developed Poiseuille flow, the local velocity inside the slot is

$$u(y) = U_s\frac{2n+1}{n+1}\left(1 + (|\,y\,|/d)^{1+1/n}\right). \tag{6.4}$$

Using $N_1 = \Psi\dot{\gamma}^{\alpha_1}$ with $\alpha_1 = 2$ and $\dot{\gamma} = \mathrm{d}u/\mathrm{d}y$, we find

$$\Delta_s = \frac{1}{a}\int_0^a N_1\,\mathrm{d}y = \frac{(2n+1)^2}{n(2+n)}\Psi\,(U_s/a)^2, \tag{6.5}$$

where the prefactor is 3 for a Boger fluid.

Now we show how to obtain the value of the mean normal stress difference Δ_1 after swelling

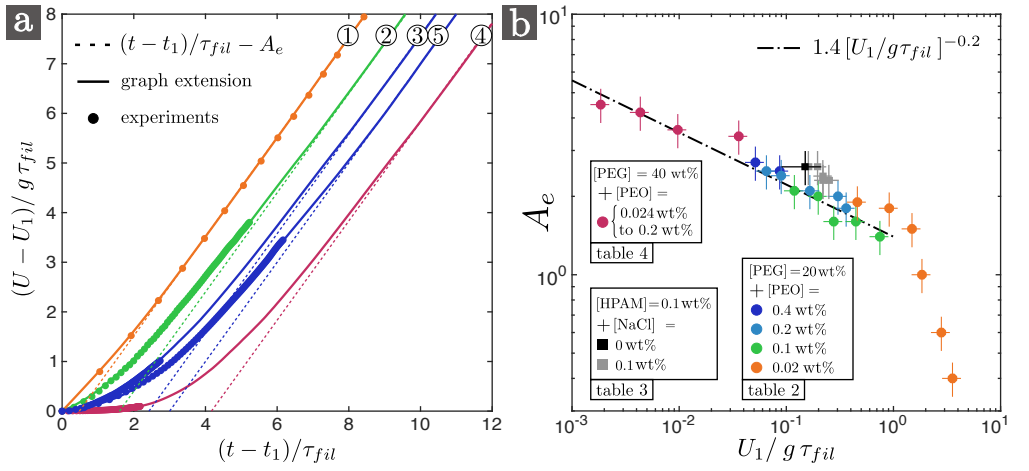

FIGURE 23. (a): $(U-U_1)/g\tau_{fil}$ versus $(t-t_1)/\tau_{fil}$, where subscript $_1$ refers to the altitude $z_1 \approx 2.5$ mm and t is the Lagrangian time (equation 5.17), for five liquids. Liquid 1: degraded ($t_d = 100$ min) 0.02 wt% PEO solution with 20 wt% PEG solvent (table 2), Liquid 2: degraded ($t_d = 60$ min) 0.1 wt% PEO solution with 20 wt% PEG solvent (table 2), Liquid 3: degraded ($t_d = 100$ min) 0.4 wt% PEO solution with 20 wt% PEG solvent (table 2), Liquid 4: 0.11 wt% PEO solution with 40 wt% PEG solvent (table 4). The curtain length L_c is 30 cm for liquids 1, 2 and 3 and is 200 cm for liquid 4. Liquid 5: liquid close to liquid 3 for $L_c = 100$ cm and observed at various vertical positions to obtain a more complete velocity field $U(z)$. The experimental data is extended with the master curve M_e (figure 20) and the free-fall regime is fitted by equation 6.6. (b): Values of A_e versus $U_1/U_e = U_1/g\tau_{fil}$ for some of the liquids of figure 20.

based on the Lagrangian force balance equation derived in §5.3. We know from figure 21.a that the extension rate goes to 0 far from the slot for an infinitely long curtain. Therefore, we can reasonably assume that the mean stress difference Δ becomes negligible in the asymptotic free-fall regime. In particular, in the free-fall regime, according to equation 5.20 where we choose to start from $z_1 \approx 2.5$ mm, the curtain velocity U reaches an oblique asymptote of equation

$$(U-U_1)/g\tau_{fil} = (t-t_1)/\tau_{fil} - A_e, \tag{6.6}$$

where

$$A_e = \Delta_1/\rho g U_1 \tau_{fil} = \Delta_1/\rho U_1 U_e = \hat{\Delta}_1/\hat{U}_1, \tag{6.7}$$

where $\hat{\Delta}_1 = \Delta_1/\Delta_e$ and $\Delta_e = \rho g z_e = \rho U_e^2 = \rho(g\tau_{fil})^2$ which is the natural scaling for Δ in the force balance equation 5.16 for a low viscosity elastic liquid. To estimate A_e, we plot $(U-U_1)/g\tau_{fil}$ as a function of $(t-t_1)/\tau_{fil}$, as shown in figure 23.a for some liquids with extensional relaxation times τ_{fil} ranging between 0.008 s and 0.68 s. We can not always observe the asymptotic free-fall regime since many curtains are either stopped before reaching it or not observed far enough from the slot. However, according to the characterisation of the flow presented in §5.4, we can use the master curve M_e identified in figure 20.a to extend the experimental curves (figure 23.a). Finally we can fit the free-fall regime by an oblic asymptote and obtain the value of A_e. In order to validate this method, we performed an additional experiment where a long curtain is observed at various vertical positions to obtain a more complete velocity field $U(z)$ for $\tau_{fil} = 0.1$ s. Unfortunately, the curtain spontaneously breaks at $z \approx 100$ cm due to the shear instability mentioned in §4.3 and we can still not observe the free-fall regime since $z_e^* \approx 120$ cm. However, the flow for $z \leqslant 100$ cm fits perfectly onto the master curve M_e, and the data presented in figure 23.a are comparable to the data corresponding to the almost same liquid observed for $z \leqslant 20$ cm, which validates the method presented here to estimate A_e.

Values of A_e are presented in figure 23.b for various solutions as a function of the dimensionless initial velocity $\hat{U}_1 = U_1/U_e$. It ranges from $A_e = 4.5$ for the solution with the largest relaxation time to negligibly small values $A_e < 0.4$ for the solutions with low extensional relaxation times which are almost immediately in the free-fall regime after leaving the slot. For $\hat{U}_1 = U_1/g\tau_{fil} \leqslant 1$, the experimental data are well captured by

$$A_e = 1.4\,\hat{U}_1^{-0.2}, \tag{6.8}$$

which, according to equation 6.7, gives finally

$$\Delta_1 \approx 1.4\,\rho g^{1.2} U_1^{0.8} \tau_{fil}^{1.2}. \tag{6.9}$$

A different behaviour is observed for $\hat{U}_1 \geqslant 1$.

As we now show, this result is analogous to Newtonian curtains for which die swell can be neglected (Tanner 2000). Since there is no internal relaxation time, the mean normal stress difference instantaneously switches from $\Delta_s = 0$ inside the slot to a value $\Delta_0 = \Delta(z=0)$ at the slot exit given by $\Delta_0 = 4\eta\,\mathrm{d}U/\mathrm{d}z(z=0)$ according to the constitutive equation. In dimensionless form, we obtain $\bar{\Delta}_0 = \bar{U}'(\bar{z}=0)$ where $\bar{\Delta} = \Delta/\Delta_v$ and $\Delta_v = \rho g z_v = \rho U_v^2 = \rho(4\eta g/\rho)^{2/3}$ is the natural scaling for Δ in the force balance equation 5.16 for a viscous Newtonian liquid. Equation 5.10 gives $\bar{\Delta}_0 = (2\bar{U}_0)^{1/2}$ for $\bar{U}_0 \ll 1$, i.e. $\Delta_0 = 2\sqrt{2}\,\rho(gU_0\eta/\rho)^{0.5}$. We can also define $A_v = \Delta_0/\rho U_0 U_v = \bar{\Delta}_0/\bar{U}_0$, and we obtain $A_v = \sqrt{2}\bar{U}_0^{-1/2}$ for $\bar{U}_0 \ll 1$ where the exponent -0.5 is larger (in absolute value) than the exponent -0.2 found in the viscoelastic case. Note that for $\bar{U}_0 \gg 1$, in which case the curtain flow is a free-fall even close to the slot, we have $\bar{\Delta}_0 = 1/\bar{U}_0$ and $A_v = \bar{U}_0^{-2}$, which is analogous to the $\hat{U}_1 \geqslant 1$ part of the curve of figure 23.b.

In order to get more more information about the physical meaning of Δ_1, we can use the integrated force balance equation 5.19 which we write here in its Eulerian form for more clarity

$$2h_1\Delta_1 - 2h\Delta = \rho q(U_1 - U) + 2\rho g \int_{z_1}^{z} h(z^*)\mathrm{d}z^*, \tag{6.10}$$

where $2h_1 = 2h(z_1) = q/U_1$. In the elastic regime $z \ll z_e$, the inertia term is negligible and the weight of the curtain between z_1 and z is supported by the difference between the contact forces $2h_1\Delta_1$ and $2h\Delta$ acting respectively on the upper and lower side. This shows that Δ_1 is the mean normal stress difference which is necessary to bear the weight of the sub-gravitational part of the curtain. We can derive the previous results by neglecting inertia and returning to the Lagrangian description. We obtain in the elastic regime $t \ll \tau_{fil}$

$$\Delta_1/U_1 - \Delta/U \approx \rho g(t - t_1). \tag{6.11}$$

Assuming that Δ becomes negligible at the transition to free-fall ($t \approx \tau_{fil}$) and that $t_1 \ll \tau_{fil}$, we find that $\Delta_1 \propto \rho g U_1 \tau_{fil}$ with a prefactor A_e which must be a decreasing function of the dimensionless initial velocity $\hat{U}_1$ since the length of the sub-gravitational part of the curtain is $z_e^* = F_e z_e$ where F_e is a decreasing function of $\hat{U}_1$. In particular, as expected from the discussion about Tanner's theory, $\Delta_1 = 0$ in the absence of gravity.

For the experiments presented so far, using equations 6.5 and 6.7, we obtain

$$\frac{\Delta_1}{\Delta_s} = \frac{n(2+n)}{(2n+1)^2}\,\frac{A_e}{\xi}\,\frac{\rho g a^2 \tau_{fil}}{U_s \Psi}. \tag{6.12}$$

Estimating A_e by the method presented in this section, we find that Δ_1/Δ_s ranges typically between 0.1 and 0.6 with no obvious trend when plotting Δ_1/Δ_s versus τ_{fil} for example. Therefore, like in the theory of Tanner, the elastic stress rapidly decreases when leaving the slot as the

polymer chains undergo a rapid strain $\varepsilon = \ln(U_1/U_s) = -\ln(\xi) < 0$ during swelling. However, in the presence of gravity, the sheet is not load-free and the swelling ratio is less than expected since some elastic stress $\Delta_1 \neq 0$ has to bear the weight of the sub-gravitational part of the curtain. In other words, the polymer chains can not recover their equilibrium shape after swelling.

The last question which remains unanswered is the link between Δ_1 and Δ_s. In the experiments presented so far, according to equations 6.5 and 6.9, both Δ_s and Δ_1 are independently affected by polymer concentration and by mechanical degradation, respectively through Ψ and τ_{fil}, in such a way that the ratio Δ_1/Δ_s is fairly constant. However, we do not know if this ratio is universal, in which case if Δ_1 would be intrinsically linked to Δ_s, or if this result is a simple coincidence. In the first case, the origin of the polymeric stress would lie in the shear deformation of the polymer chains in the slot, in which case the length z_e^* of the sub-gravitational regime would be a function of Δ_s. In particular, a curtain of vanishing slot velocity U_s would exhibit no sub-gravitational elastic regime although $U_1 \ll g\tau_{fil}$ since Δ_s, and therefore Δ_1, would be arbitrarily small. To answer this question, we need to compare the flow of two curtains made of the same liquid but with radically different values of Δ_s. According to equations 6.5 and 6.9, changing the slot thickness $2a$ while keeping the same initial velocity U_1 is a good solution: if Δ_1 does not change while Δ_s changes, it means that the description of the flow provided in 5.4 is universal and that the master curve M_e does not depend on the history of the polymer chains upstream of the curtain.

6.3. *The influence of the die geometry*

In order to check if Δ_1 is intrinsically linked to Δ_s or not, i.e. whether or not the curtain flow affected by the history of polymer deformations upstream of the curtain, we compare the flow of two curtains of same length and made of the same liquid (table 5). The first curtain is extruded from the slot die of figure 1.b where the slot thickness $2a = 1$ mm. The flow rate is $q = 1.4$ cm^2/s, the mean velocity is $U_s = q/2a = 0.14$ m/s in the slot and $U_1 = 0.085$ m/s at $z_1 = 2.5$ mm from the slot exit, after an initial swelling of ratio $\xi = U_s/U_1 = 1.6 > 1$. The second curtain is formed using a second "die" presented in figure 24.a where the liquid flows freely along an inclined plane before forming a vertical curtain when falling off the edge. Imposing a flow rate $q^\star = 0.85$ cm^2/s $< q$, we measure that the thickness of the liquid layer flowing down the plane is $2a^\star = 2.5$ mm $> 2a$, which gives a mean velocity $U_s^\star = q^\star/2a^\star = 0.034$ m/s $< U_s$. We measure that the mean vertical velocity is $U_1^\star = 0.088$ m/s $\approx U_1$ at 3 mm from the edge of the plane. Therefore, the thickness of the liquid rapidly decreases by a factor $\xi^\star = U_s^\star/U_1^\star = 0.39 < 1$ at the edge of the plane.

As presented in figure 24.b, the flows of these two curtains are slightly different. The liquid velocity, which is initially comparable since $U_1^\star \approx U_1$, increases a bit faster when falling off the edge of the plane than when being extruded from the slot. For example, the liquid acceleration is respectively 5.5 m/s^2 and 4.6 m/s^2 at $z = 18$ cm. Therefore, the flow of the curtain falling of the inclined plane does not perfectly collapse on the master curve M_e identified in figure 20.a. Let us estimate Δ_s and Δ_1 for these two curtains.

We find $\Delta_s \approx 1400$ Pa for the slot die. For the inclined plane, we estimate the mean normal stress difference $\Delta_s^\star$ developed by the liquid when flowing down the plane using equation 6.5 where a is replaced by $2a^\star$ since the flow is a semi-Poiseuille. We find $\Delta_s^\star \approx 3.3$ Pa which is much less than Δ_s. Hence, this change in die geometry reduces the elastic stress upstream of the curtain by a factor $\Delta_s^\star/\Delta_s \approx 2 \times 10^{-3} \ll 1$. This result suggests that the effect of Δ_s on the curtain flow identified in figure 24.b in actually very weak. Indeed, despite a much different flow upstream of the curtain, the curtain flows are quite comparable. In particular, $z_e = g\tau_{fil}^2$ is still the appropriate scaling for the length of the sub-gravitational regime. Therefore, the mean normal stress difference Δ_1 developed a few millimetres below slot or below the edge of the plane respectively must be comparable in both experiments. Using the method described in §6.2, we

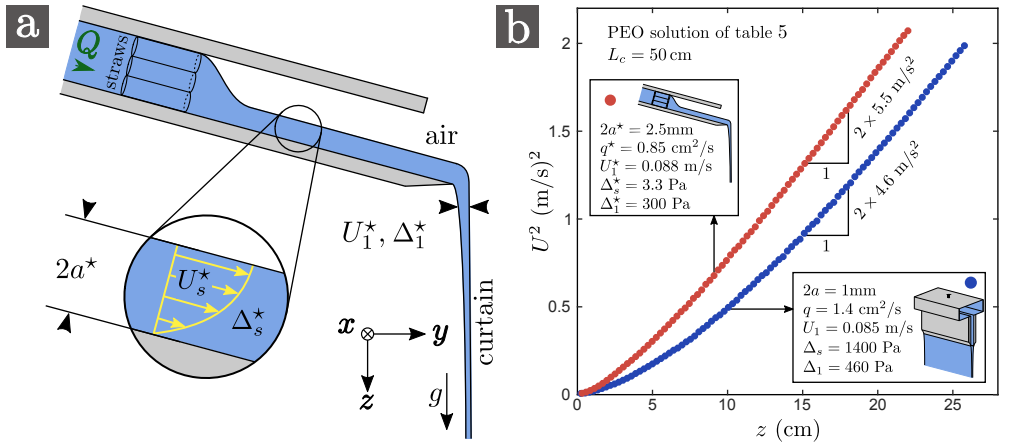

FIGURE 24. (a): Sketch of a curtain formed when a liquid layer of thickness $2a^\star$ falls off the edge of an inclined plane with mass flow Q. A grid of straws is used to homogenise the flow in the x direction and the linear flow rate is $q = Q/\rho l$ where l is the curtain width. Guides are used to avoid sheet retraction. (b): Using the PEO solution of table 5, comparison of the squared velocity field $U^2(z)$ of the curtain formed using the inclined plane and using the slot die of figure 1.*b*. Both curtains start with comparable initial velocities U_1 and share the same length $L_c = 50$ cm. The polymeric mean normal stress difference Δ_s upstream of the curtain is 1400 Pa for the slot die but only 3.3 Pa for the inclined plane.

find $A_e \approx 3.4$ for the slot die and $A_e^\star \approx 2.1$ for the inclined plane. In the latter case, note that this estimation is based on comparisons with other curtain flows from the slot die since the master curve can not be used to extend the experimental data. We find respectively $\Delta_1 \approx 460$ Pa and $\Delta_1^\star \approx 300$ Pa which are indeed comparable, i.e. $\Delta_1^\star/\Delta_1 \approx 0.6$. For the slot die, the polymeric stress decreases during swelling and $\Delta_1/\Delta_s \approx 0.3 < 1$. However, for the inclined plane, the polymeric stress increases during the contraction at the edge of the plane and $\Delta_1^\star/\Delta_s^\star \approx 90 > 1$. In fact, in both cases, the polymer molecules undergo a rapid strain $\varepsilon = \ln(U_1/U_s)$ which is $-0.50 < 0$ for the slot and which is $0.95 > 0$ for the inclined plane. According to figure 6, such strains can indeed cause significant modifications of the polymeric stress.

To summarise, the mean normal stress difference switches from a value Δ_s inside the die to a value Δ_1 at the die exit, where Δ_1 is of order $\rho g U_1 \tau_{fil}$ independently of the flow history inside the die, with a prefactor A_e which is a decreasing function of the initial velocity. However, since the flow is slightly modified when changing Δ_s, the prefactor also depends on the die geometry and is an increasing function of Δ_s. The length z_e^* of the sub-gravitational regime is of order $g\tau_{fil}^2$ with a prefactor F_e which is a decreasing function of the initial velocity and which is also an increasing function of Δ_s. These results suggest that the polymeric stress Δ does not come from the shear deformation of the polymer chains in the die but rather comes from a rapid extensional stretching of the polymer chains when leaving the die.

Hence, we can now propose a universal mechanism for the transition from the elastic regime to the free-fall regime. After initial stretching at the die exit, the polymer molecules exhibit strong elastic stresses which are initially balanced by gravity in the elastic regime. As the polymer molecules are advected by the flow, elastic forces decrease since the extension rate $\dot{\varepsilon} = \mathrm{d}U/\mathrm{d}z$ decreases, until gravity is mostly balanced by inertia at the transition to the free-fall regime where $\dot{\varepsilon} \sim \sqrt{g/z}$. Elastic stresses are expected to become negligible when the extension rate $\dot{\varepsilon}$ becomes less than $1/\tau_{fil}$, i.e. when the rate of stretching exerted by the flow no longer overcomes the relaxation of polymer molecules, which gives a transition length of order $g\tau_{fil}^2 = z_e$.

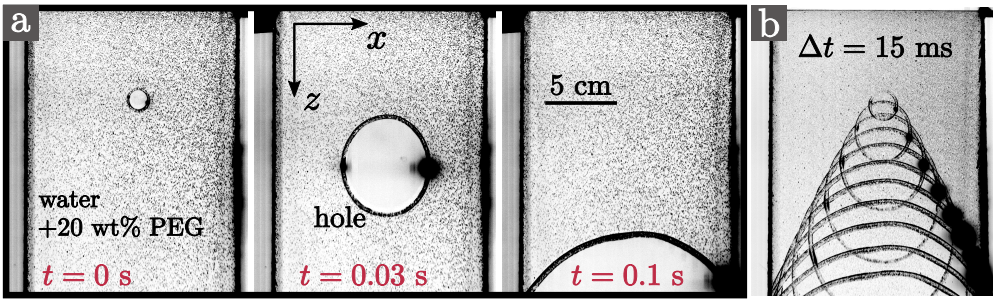

FIGURE 25. (a): Time evolution of a hole forming spontaneously in a curtain of 20 wt% PEG solvent with flow rate $q = 3.3$ cm^2/s and length $L_c = 30$ cm. The hole is advected by the flow (self-healing). (b): Image superposition.

7. Curtain stability

In this section, we investigate the influence of elasticity on the stability of the curtain in terms of spontaneous hole opening events. The unstable curtain flows described in §4.2 are not considered in this section.

7.1. *Dynamics of hole opening*

In figures 25.a and 25.b, we show the time evolution of a hole forming spontaneously in a Newtonian curtain of 20 wt% PEG solvent. Such a hole can be generated by impurities in the liquid such as bubbles which are inevitably generated in the hydraulic loop. The hole in figure 25 is advected by the flow while growing in size and the liquid is collected in a rim. According to Taylor (1959) and Culick (1960), if capillary forces are only balanced by inertia, the local retraction speed of the hole in the reference frame of the moving liquid is

$$V = \sqrt{\gamma/\rho h}, \tag{7.1}$$

where ρ and γ are the liquid density and surface tension and $h(z)$ is the local half thickness of the curtain. In the case of a Newtonian liquid of dynamic viscosity η, Savva & Bush (2009) showed that the retraction speed of a hole initiated in a motionless sheet of constant thickness goes from 0 to V in a time which increases as the Ohnesorge numbers $Oh = \eta/(4h\rho\gamma)^{1/2}$ increases. Capillary forces are initially balanced by viscous forces before inertia finally dominates. Based on similar results, Sünderhauf *et al.* (2002) concluded that increasing the liquid viscosity stabilises the curtain since the dynamics of hole opening is slowed down temporarily. Karim *et al.* (2018*b*) recently measured the retraction speed of holes opening spontaneously in curtains of low-viscosity Boger PEO solutions. They report that the ratio of the local retraction speed to the local Taylor-Culick velocity decreases when the local Ohnesorge number increases for Oh ranging between 0.22 and 0.43. This ratio was 0.95 for the solution with the highest extensional relaxation time $\tau_{fil} = 0.16$ s and the authors conclude that elastic stresses slow down the hole opening process.

In the case where both viscous and elastic effects can be neglected, the part of the liquid rim corresponding to the upper edge of the hole retracts at velocity $V - U$ in the reference frame of the laboratory, where V is calculated based on the local curtain thickness $2h(z)$ and where $U(z)$ is the local velocity of the surrounding liquid. This local competition can be written in terms of a Weber number

$$We = \left(\frac{U}{V}\right)^2 = \frac{\rho h U^2}{\gamma} = \frac{\rho q U}{2\gamma}, \tag{7.2}$$

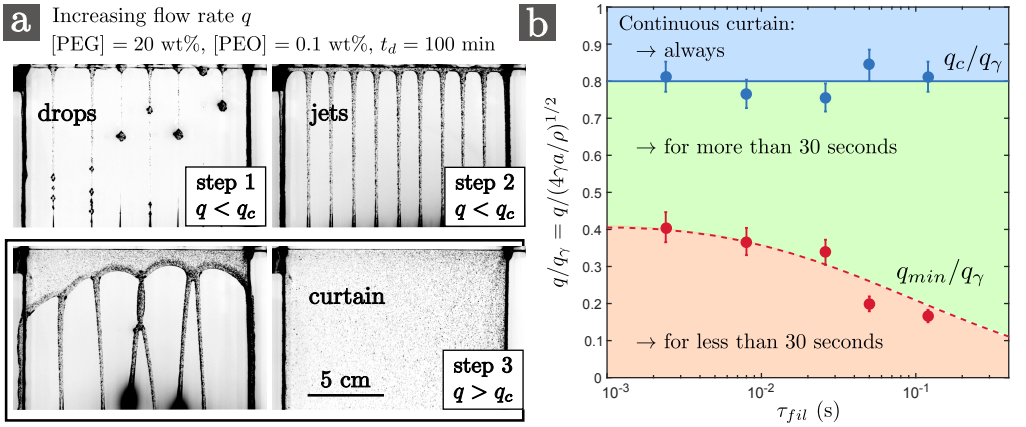

FIGURE 26. (a): Different regimes observed when increasing the flow rate from 0 to 6 cm^2/s for the degraded (t_d = 100 min) 0.1 wt% PEO solution with 20 wt% PEG solvent (table 2). (b): Critical flow rate q_c (above which any hole is advected by the flow) and minimum flow rate q_{min} (required to maintain a continuous curtain for more than 30 seconds), divided by $q_\gamma = (4a\gamma/\rho)^{1/2}$, against the extensional relaxation time τ_{fil} for the five degraded (t_d = 100 min) PEO solutions with 20 wt% PEG solvent (table 2). $q_\gamma = 3.5$ cm^2/s and curtain length is $L_c = 30$ cm.

which can be less than one close to the slot and become larger than one downstream. Therefore, if a hole opens at an altitude where $We > 1$, i.e. where advection is faster than the hole opening process, it will be carried away by the flow, like in figure 25. This process is often referred to as self-healing. However, if a hole opens in the unstable part of the curtain where $We < 1$, the upper edge of the hole propagates upwards and stops when reaching the slot whereas the lower end propagates downwards, in which case the curtain is finally split into two parts delimited by a rim which takes the form of an arch. The latter scenario is not possible if the Weber number is larger than one everywhere, i.e. if the initial velocity $U_s = q/2a$ at the slot exit is larger than the value of V at the slot exit. Equivalently, the linear flow rate q has to be larger than a critical value

$$q_\gamma = (4a\gamma/\rho)^{1/2}. \tag{7.3}$$

This description does not take die swell into account and one could argue that U_1 is the velocity which has to be larger than V. This gives a larger critical flow rate $q_\gamma = (4a\xi\gamma/\rho)^{1/2}$ where $\xi = U_s/U_1$ is the die swell ratio.

7.2. *Critical flow rate*

In figure 26.a, we show the different regimes observed when increasing the flow rate. First (step 1), droplets are periodically emitted from equally spaced spots along the slot. In the case of a polymer solution, these drops can be connected by filaments (Clasen *et al.* 2009). Then, the liquid falls in the form of equally spaced continuous jets (step 2). The transition from dripping to jetting is described by Clanet & Lasheras (1999) in the case of a single jet issuing from a nozzle. The distance between two jets is typically captured by the value $2\pi\sqrt{2}(\gamma/\rho g)^{1/2} = 2.2$ cm expected from the Rayleigh-Taylor instability theory (Fermigier *et al.* 1992; Brunet *et al.* 2007). As the flow rate is further increased, neighbouring jets merge and form thicker jets until the arches are finally advected and a continuous sheet of liquid suddenly emerges from the slot (step 3) at a critical flow rate q_c which is measured. Values of the ratio q_c/q_γ are reported in figure 26.b for the five degraded (t_d = 100 min) PEO solutions with 20 wt% PEG solvent (table 2). Results are reproducible and are plotted against the extensional relaxation time τ_{fil}. We measure that $q_c/q_\gamma \approx 0.8$ for all solutions. This shows that the archs indeed detach from the slot when the

extrusion velocity becomes of the order of the Taylor-Culick velocity and suggests that elastic forces have a negligible influence on the retraction speed of the hole. The discrepancy may be due to the weight of the rim which pulls archs downwards. Rim weight effects in liquid curtains are for example discussed by Roche *et al.* (2006). Taking die swell into account, we obtain a value of q_c/q_γ closer to 0.7.

7.3. *Minimum flow rate*

Starting from $q > q_c$, nothing special happens when decreasing the flow rate below q_c and the curtain generally remains continuous for a long time. However, since holes are continuously generated in the curtain, the curtain will finally break when a hole eventually opens close enough to the slot where $We < 1$, i.e. where the upper edge of a hole propagates upwards. Hence, as proposed by Becerra & Carvalho (2011), we define the minimum flow rate q_{min} above which the liquid sheet remains continuous for more than a certain amount of time, for example 30 seconds since liquid deposition on a substrate takes a few seconds in curtain coating. We measure q_{min} as follows. Starting from a continuous curtain, the flow rate q is decreased step by step, each step lasting 30 seconds, until the curtain breaks at $q = q_{min}$. We obtain reproducible values of q_{min}. The ratio q_{min}/q_γ is reported in figure 26.b. Values of q_{min} decrease from 1.3 cm^2/s for the 0.004 wt% PEO solution, which is also the value measured with the pure solvent, to 0.58 cm^2/s for the 0.4 wt% PEO solution, i.e. q_{min} decreases by a factor 2.2. Therefore, curtain coating can be performed at lower flow rates when adding polymer molecules to the liquid, as already shown by Becerra & Carvalho (2011) and Karim *et al.* (2018*b*) with similar measurements.

The value of q_{min} is linked to the frequency of spontaneous hole opening events in the curtain. Holes are mostly generated far from the slot where the curtain is thin. Curtain are indeed often continuous close to the slot but constantly punctured downstream, as is commonly observed in water fountains. The frequency of hole opening events must depend on the concentration of impurities in the liquid, which is not controlled in our experiment. We measure that this frequency decreases when increasing the extensional relaxation time of the solution. Typically, for the 0.02 wt% PEO solution with 20 wt% PEG solvent (table 2) extruded at flow rate $q = 1.7$ cm^2/s with curtain length $L_c = 30$ cm, the frequency of spontaneous hole opening events decreases from about one hole per minute before degradation ($t_d = 0$ min) to ten holes per second after $t_d = 100$ minutes of degradation, most of them being generated more than 10 cm below the slot. In the latter case, the velocity field $U(z)$ for $z < 20$ cm can only be measured after raising the flow rate to 3.4 cm^2/s. Indeed, the hole opening frequency decreases when increasing the flow rate since the curtain becomes thicker everywhere.

We conclude that polymer addition greatly enhances the stability of the curtain. This result can be interpreted as a greater resistance of the liquid sheet to bubble bursting within the liquid. We speculate that two liquid layers separating a bubble on both sides from the ambient air undergo an extensional flow and are therefore more difficult to break due to the elastic stresses arising from the stretching of polymer molecules, like in the filament thinning experiment where breaking is inhibited by the presence of polymer molecules. This interpretation is consistent with the experiments conducted by Karim *et al.* (2018*b*) which consist of applying a local disturbance on the curtain with an air jet blown through a needle. Indeed, since Newtonian curtains break much more easily than viscoelastic curtains, the authors concluded that the growth rate of any disturbance leading to the formation of a hole is delayed by polymer addition.

8. Summary and discussion

In this paper, we present the first intensive experimental investigation of the role of elasticity in the extensional flow of a sheet - or curtain - of low-viscosity liquid falling freely from a slot at constant flow rate. Contrary to film casting, gravity is the only source of axial tension. The mean

liquid velocity $U(z)$, where z is the distance from the slot exit, is measured for polymer solutions with various rheological behaviours. We show that the flow is only influenced by the value of the extensional relaxation time τ_{fil} measured with a CaBER rheometer. If the liquid initial velocity U_1 after swelling is such that $U_1 \ll g\tau_{fil}$, gravity is initially balanced by the elastic stresses arising from the stretching of polymer molecules. In this elastic regime, the liquid acceleration $U\mathrm{d}U/\mathrm{d}z$ is less than the gravitational acceleration g. However, inertia finally dominates over elasticity far from the slot and the liquid acceleration reaches the asymptotic free-fall value g. The length of the sub-gravitational part of the curtain is $z_e^* = F_e z_e$ where $z_e = g\tau_{fil}^2$ and where F_e is a decreasing function of $U_1/g\tau_{fil}$. In particular, the flow is a free-fall even close to the slot if $U_1 \gg g\tau_{fil}$. When considering the flow far from the impingement zone, we show that the velocity field $U(z)$ rescales on a master curve, like for Newtonian liquids of dynamic viscosity η and density ρ where the flow is initially dominated by viscous dissipation if the initial velocity is less than $U_v = \sqrt{gz_v}$ where $z_v = ((4\eta/\rho)^2/g)^{1/3}$. We show that the flow is only weakly influenced by the history of polymer deformations in the die upstream of the curtain. In particular, the mean normal stress difference Δ switches from a shear value Δ_s inside the slot to an extensional value $\Delta_1 = A_e \rho g U_1 \tau_{fil}$ after swelling which is needed to bear the weight of the sub-gravitational part of the curtain, where A_e is a decreasing function of $U_1/g\tau_{fil}$ and also depends on Δ_s. Hence, F_e also depends on Δ_s. Furthermore, we show that polymer addition reduces the minimum flow rate required to maintain a continuous curtain and greatly diminishes the frequency of spontaneous hole opening events.

We thank Henri Lhuissier for many enlightening discussions, as well as Julien Beaumont from Saint-Gobain Recherche who brought this topic to the lab. We also thank Alain Ponton for his assistance with shear rheology measurements, as well as Mathieu Receveur, Laurent Réa, Yann Le Goas and Arnaud Grados for their technical assistance.

Appendix A. Rheology of curtain solutions

REFERENCES

ABRAMOWITZ, M. & STEGUN, I. A. 1964 *Handbook of mathematical functions: with formulas, graphs, and mathematical tables*, , vol. 55. Courier Corporation.

AIDUN, C. K. 1987 Mechanics of a free-surface liquid film flow. *Journal of applied mechanics* **54** (4), 951–954.

ALAIE, S. M. & PAPANASTASIOU, T. C. 1991 Film casting of viscoelastic liquid. *Polymer Engineering & Science* **31** (2), 67–75.

AMAROUCHENE, Y., BONN, D., MEUNIER, J. & KELLAY, H. 2001 Inhibition of the finite-time singularity during droplet fission of a polymeric fluid. *Physical Review Letters* **86** (16), 3558.

ANNA, S. L. & MCKINLEY, G. H. 2001 Elasto-capillary thinning and breakup of model elastic liquids. *Journal of Rheology* **45** (1), 115–138.

BECERRA, M. & CARVALHO, M. S. 2011 Stability of viscoelastic liquid curtain. *Chemical Engineering and Processing: Process Intensification* **50** (5), 445–449.

BIRD, R. B., ARMSTRONG, R. C. & HASSAGER, O. 1987 Dynamics of polymeric liquids. vol. 1: Fluid mechanics .

BROWN, D. R. 1961 A study of the behaviour of a thin sheet of moving liquid. *Journal of fluid mechanics* **10** (2), 297–305.

BRUNET, P., FLESSELLES, J-M. & LIMAT, L. 2007 Dynamics of a circular array of liquid columns. *The European Physical Journal B* **55** (3), 297–322.

CARTALOS, U. & PIAU, J. M. 1992 Creeping flow regimes of low concentration polymer solutions in thick solvents through an orifice die. *Journal of non-newtonian fluid mechanics* **45** (2), 231–285.

CHEN, E. B., MORALES, A. J., CHEN, C. C., DONATELLI, A. A., BANNISTER, W. W. & CUMMINGS,

[PEO] wt %	t_d min	η_0 Pa.s	η_p Pa.s	n	$1/\dot{\gamma}_c$ s	α_1	Ψ Pa.s$^{\alpha_1}$	τ_{fil} s	η_E Pa.s	b	Wi	U_s m/s	U_1 m/s
0.004	0	0.017	0.001	1.0				0.010	1×10^2	5×10^4	1.1	0.22	0.20
-	10	0.017	0.001	1.0				0.0073	7×10^1	3×10^4	0.83	0.29	0.26
-	20	0.017	0.001	1.0				0.0050	5×10^1	2×10^4	0.57	0.33	0.29
-	40	0.017	0.001	1.0				0.0036	3×10^1	1×10^4	0.41	0.32	0.28
-	60	0.017	0.001	1.0				0.0029	3×10^1	1×10^4	0.33	0.32	0.27
-	100	0.017	0.001	1.0				0.0024	2×10^1	1×10^4	0.27	0.33	0.28
0.02	0	0.019	0.002	1.0				0.060	4×10^2	1×10^5	6.5	0.38	0.27
-	10	0.019	0.002	1.0				0.030	2×10^2	5×10^4	3.3	0.34	0.27
-	20	0.019	0.002	1.0				0.018	2×10^2	5×10^4	2.0	0.34	0.26
-	40	0.019	0.002	1.0				0.015	1×10^2	2×10^4	1.6	0.34	0.27
-	60	0.019	0.002	1.0				0.010	1×10^2	2×10^4	1.1	0.34	0.27
-	100	0.019	0.002	1.0				0.008	1×10^2	2×10^4	0.87	0.34	0.28
0.1	0	0.037	0.020	0.96	0.14	2	0.0063	0.23	1×10^3	2×10^4	20	0.26	0.14
-	10	0.035	0.018	0.95	0.13	2	0.0030	0.15	8×10^2	2×10^4	13	0.29	0.17
-	20	0.034	0.017	0.95	0.11	2	0.0007	0.085	6×10^2	2×10^4	7.6	0.25	0.17
-	40	0.030	0.013	0.96	0.050	2	0.0004	0.064	6×10^2	2×10^4	6.0	0.25	0.17
-	60	0.029	0.012	0.96	0.029	2	0.0003	0.041	3×10^2	1×10^4	3.9	0.25	0.18
-	100	0.029	0.012	0.95	0.025	2	0.0002	0.026	3×10^2	1×10^4	2.5	0.25	0.19
0.2	0	0.12	0.10	0.85	1.3	2	0.013	0.28	2×10^3	1×10^4	17	0.21	0.12
-	10	0.084	0.067	0.88	0.50	2	0.007	0.20	1×10^3	1×10^4	13	0.23	0.13
-	20	0.075	0.058	0.88	0.33	2	0.004	0.15	1×10^3	1×10^4	10	0.25	0.13
-	40	0.063	0.046	0.90	0.25	2	0.002	0.10	1×10^3	1×10^4	7.3	0.27	0.16
-	60	0.054	0.037	0.91	0.10	2	0.001	0.06	6×10^2	1×10^4	4.6	0.30	0.18
-	100	0.053	0.036	0.91	0.083	2	0.0003	0.05	6×10^2	1×10^4	3.9	0.29	0.18
0.4	0	1.2	1.2	0.62	6.7	2	0.13	1.2	6×10^3	3×10^3	33	0.17	0.089
-	10	0.68	0.66	0.67	2.5	2	0.04	0.51	3×10^3	2×10^3	17	0.19	0.097
-	20	0.48	0.46	0.69	1.4	2	0.02	0.38	2×10^3	2×10^3	14	0.16	0.088
-	40	0.33	0.31	0.72	0.71	2	0.008	0.26	2×10^3	3×10^3	11	0.19	0.10
-	60	0.25	0.23	0.74	0.40	2	0.006	0.20	2×10^3	4×10^3	9.2	0.18	0.10
-	100	0.20	0.18	0.77	0.29	2	0.004	0.12	1×10^3	3×10^3	6.0	0.17	0.10

TABLE 2. Rheological parameters of the PEO solutions with 20 wt% PEG solvent used in curtain experiments, where t_d is the time of degradation. The first columns are similar to table 1 and the solvent viscosity is $\eta_s = 0.017$ Pa.s. Wi is the Weissenberg number (equation 5.29), $U_s = q/2a$ is the extrusion velocity where q is the linear flow rate, and $U_1 = U(z_1)$ is the liquid velocity measured at $z_1 \approx 2.5$ mm from the slot, i.e. after swelling.

B. T. 1998 Fluorescein and poly (ethylene oxide) hose stream additives for improved firefighting effectiveness. *Fire Technology* **34** (4), 291–306.

CHEN, P., YAO, L., LIU, Y., LUO, J., ZHOU, G. & JIANG, B. 2012 Experimental and theoretical study of dilute polyacrylamide solutions: effect of salt concentration. *Journal of molecular modeling* **18** (7), 3153–3160.

CLANET, C. & LASHERAS, J. C. 1999 Transition from dripping to jetting. *Journal of fluid mechanics* **383**, 307–326.

CLARKE, N. S. 1966 A differential equation in fluid mechanics. *Mathematika* **13** (1), 51–53.

CLARKE, N. S. 1968 Two-dimensional flow under gravity in a jet of viscous liquid. *Journal of Fluid Mechanics* **31** (3), 481–500.

[NaCl] (wt %)	t_d min	η_0 (Pa.s)	η_p (Pa.s)	n	$1/\dot{\gamma}_c$ (s)	α_1	Ψ (Pa.s$^{\alpha_1}$)	τ_{fil} (s)	η_E (Pa.s)	b	Wi	U_s (m/s)	U_1 (m/s)
0	0	1×10^2	1×10^2	0.20	8×10^2	0.81	3.09	0.4	4×10^3	1×10^1	2	0.29	0.29
-	10	1×10^2	1×10^2	0.20	8×10^2	0.92	1.38	0.4	2×10^3	7×10^0	2	0.31	0.30
-	20	1×10^2	1×10^2	0.20	8×10^2	0.88	1.82	0.3	1×10^3	3×10^0	2	0.31	0.31
-	40	1×10^2	1×10^2	0.20	8×10^2	0.86	2.00	0.3	1×10^3	3×10^0	2	0.28	0.31
-	60	1×10^2	1×10^2	0.20	8×10^2	1.00	0.85	0.3	1×10^3	3×10^0	1	0.29	0.31
-	100	1×10^2	1×10^2	0.20	8×10^2	0.99	0.87	0.2	1×10^3	3×10^0	1	0.31	0.31
0.1	0	0.61	0.61	0.49	2×10^1	1.1	0.42	0.24	1×10^3	8×10^2	8.2	0.33	0.33
-	10	0.61	0.61	0.49	2×10^1	1.1	0.35	0.19	8×10^2	7×10^2	6.5	0.28	0.30
-	20	0.61	0.61	0.49	2×10^1	1.1	0.28	0.16	8×10^2	7×10^2	5.4	0.29	0.30
-	40	0.61	0.61	0.49	2×10^1	1.1	0.34	0.15	8×10^2	7×10^2	5.1	0.29	0.32
-	60	0.61	0.61	0.49	2×10^1	1.1	0.36	0.14	5×10^2	4×10^2	4.8	0.28	0.30
-	100	0.61	0.61	0.49	2×10^1	1.1	0.27	0.12	5×10^2	4×10^2	4.1	0.27	0.29
0		1×10^2	1×10^2	0.20	8×10^2	0.84	2.5	0.5	1×10^3	3×10^0	2	0.12	0.12
0.01		8×10^1	8×10^1	0.25	8×10^2	0.83	2.4	0.4	8×10^2	5×10^0	2	0.13	0.12
0.1		0.70	0.70	0.47	20	0.95	0.83	0.19	5×10^2	4×10^2	6.2	0.13	0.14
1		0.025	0.024	0.71	0.71	1.2	0.11	0.077	6×10^2	1×10^4	7.6	0.12	0.12
10		0.0088	0.0078	0.81	0.25	1.6	0.0063	0.050	4×10^2	3×10^4	7.0	0.14	0.13

TABLE 3. Rheological parameters of the salted (NaCl) HPAM solutions used in curtain experiments, where t_d is the time of degradation (top) which is unknown for the last liquid (bottom) where salt is added after each PIV measurement. The first columns are similar to table 1 and the solvent viscosity is $\eta_s = 0.001$ Pa.s. Wi is the Weissenberg number (equation 5.29), $U_s = q/2a$ is the extrusion velocity where q is the linear flow rate, and $U_1 = U(z_1)$ is the liquid velocity measured at $z_1 \approx 2.5$ mm from the slot, i.e. after swelling.

[PEO] (wt %)	η_0 (Pa.s)	η_p (Pa.s)	n	$1/\dot{\gamma}_c$ (s)	α_1	Ψ (Pa.s$^{\alpha_1}$)	τ_{fil} (s)	η_E (Pa.s)	b	Wi	U_s (m/s)	U_1 (m/s)
0.2	0.70	0.55	0.90	2.0	2	0.26	1.1	7×10^3	6×10^3	37	0.040	0.020
0.11	0.35	0.20	0.95	0.56	2	0.12	0.68	4×10^3	1×10^4	28	0.057	0.029
0.048	0.21	0.06	1		2	0.032	0.42	2×10^3	2×10^4	21	0.073	0.040
0.024	0.17	0.02	1		2	0.004	0.17	9×10^2	2×10^4	9.1	0.098	0.060

TABLE 4. Rheological parameters of the PEO solutions with 40 wt% PEG solvent used in curtain experiments. The first columns are similar to table 1 and the solvent viscosity is $\eta_s = 0.15$ Pa.s. Wi is the Weissenberg number (equation 5.29), $U_s = q/2a$ is the extrusion velocity where q is the linear flow rate, and $U_1 = U(z_1)$ is the liquid velocity measured at $z_1 \approx 2.5$ mm from the slot, i.e. after swelling.

CLASEN, C., BICO, J., ENTOV, V. M. & MCKINLEY, G. H. 2009 Gobbling drops: the jetting–dripping transition in flows of polymer solutions. *Journal of fluid mechanics* **636**, 5–40.

CLASEN, C., PLOG, J. P., KULICKE, W.-M, OWENS, M., MACOSKO, C., SCRIVEN, L. E., VERANI, M. & MCKINLEY, G. H. 2006 How dilute are dilute solutions in extensional flows? *Journal of Rheology* **50** (6), 849–881.

CROOKS, R. & BOGER, D. V. 2000 Influence of fluid elasticity on drops impacting on dry surfaces. *Journal of Rheology* **44** (4), 973–996.

CULICK, F. E. C. 1960 Comments on a ruptured soap film. *Journal of applied physics* **31** (6), 1128–1129.

[PEG] wt %	[PEO] wt %	η_0 Pa.s	η_p Pa.s	n	$1/\dot{\gamma}_c$ s	α_1	Ψ Pa.s$^{\alpha_1}$	τ_{fil} s	η_E Pa.s	b	Wi
20	0.4	0.21	0.19	0.81	0.4	2	0.006	0.16	1×10^3	3×10^3	7.8

TABLE 5. Rheological properties of the liquid used as a reference for the investigations on die swell (§4.6 and §6.1), and on the role of flow rate (§4.4) and die geometry (see §6.3). All these experiments are performed the same day. This liquid is close to (but not exactly the same as) the degraded ($t_d = 100$ min) 0.4 wt% PEO solution with 20 wt% PEG solvent presented in table 2. Density is $\rho = 1026$ kg/m^3, surface tension is $\gamma = 62$ mN/m, solvent viscosity is $\eta_s = 0.017$ Pa.s and Wi is the Weissenberg number (equation 5.29)

DAERR, A. & MOGNE, A. 2016 Pendent_drop: an imagej plugin to measure the surface tension from an image of a pendent drop. *Journal of Open Research Software* **4** (1).

DOMBROWSKI, N. & JOHNS, W. R. 1963 The aerodynamic instability and disintegration of viscous liquid sheets. *Chemical Engineering Science* **18** (3), 203–214.

DONTULA, P., MACOSKO, C. W. & SCRIVEN, L. E. 1998 Model elastic liquids with water-soluble polymers. *AIChE journal* **44** (6), 1247–1255.

EGGERS, J. 2014 Instability of a polymeric thread. *Physics of Fluids* **26** (3), 033106.

EWOLDT, R. H., JOHNSTON, M. T. & CARETTA, L. M. 2015 Experimental challenges of shear rheology: how to avoid bad data. In *Complex Fluids in Biological Systems*, pp. 207–241. Springer.

FERMIGIER, M., LIMAT, L., WESFREID, J. E., BOUDINET, P. & QUILLIET, C. 1992 Two-dimensional patterns in rayleigh-taylor instability of a thin layer. *Journal of Fluid Mechanics* **236**, 349–383.

GRAESSLEY, W. W. 1980 Polymer chain dimensions and the dependence of viscoelastic properties on concentration, molecular weight and solvent power. *Polymer* **21** (3), 258–262.

GUGLER, G., BEER, R. & MAURON, M. 2010 Coatability of viscoelastic liquid curtain. In *Proceedings of the 15th international coating science and technology symposium, St. Paul , Minnesota*.

HUANG, D. C. & WHITE, J. L. 1979 Extrudate swell from slit and capillary dies: an experimental and theoretical study. *Polymer Engineering & Science* **19** (9), 609–616.

KARIM, A. M., SUSZYNSKI, W. J., FRANCIS, L. F. & CARVALHO, M. S. 2018*a* Effect of viscosity on liquid curtain stability. *AIChE Journal* **64** (4), 1448–1457.

KARIM, A. M., SUSZYNSKI, W. J., GRIFFITH, W. B., PUJARI, S., FRANCIS, L. F. & CARVALHO, M. S. 2018*b* Effect of viscoelasticity on stability of liquid curtain. *Journal of Non-Newtonian Fluid Mechanics* **257**, 83–94.

KAYS, W. M., CRAWFORD, M. E. & WEIGAND, B. 2005 *Convective heat and mass transfer*.

MACOSKO, C. W. 1994 *Rheology: principles, measurements, and applications*. Wiley-vch.

MCKINLEY, G. H. 2005 Visco-elasto-capillary thinning and break-up of complex fluids. *Annual Rheological Review* **3**, 1–48.

MIYAMOTO, K. & KATAGIRI, Y. 1997 Curtain coating. In *Liquid film coating*, pp. 463–494. Springer.

PAPANASTASIOU, T. C., MACOSKO, C. W., SCRIVEN, L. E. & CHEN, Z. 1987 Fiber spinning of viscoelastic liquid. *AIChE journal* **33** (5), 834–842.

RAMOS, J. I. 1996 Planar liquid sheets at low reynolds numbers. *International journal for numerical methods in fluids* **22** (10), 961–978.

RICHARDSON, S. 1970 The die swell phenomenon. *Rheologica Acta* **9** (2), 193–199.

ROCHE, J. S., GRAND, N. LE, BRUNET, P., LEBON, L. & LIMAT, L. 2006 Pertubations on a liquid curtain near break-up: Wakes and free edges. *Physics of fluids* **18** (8), 082101.

ROTHSTEIN, J. P. & MCKINLEY, G. H. 1999 Extensional flow of a polystyrene boger fluid through a 4: 1: 4 axisymmetric contraction/expansion. *Journal of non-newtonian fluid mechanics* **86** (1), 61–88.

SATOH, N., TOMIYAMA, H. & KAJIWARA, T. 2001 Viscoelastic simulation of film casting process for a polymer melt. *Polymer Engineering & Science* **41** (9), 1564–1579.

SATTLER, R., GIER, S., EGGERS, J. & WAGNER, C. 2012 The final stages of capillary break-up of polymer solutions. *Physics of Fluids* **24** (2), 023101.

SATTLER, R., WAGNER, C. & EGGERS, J. 2008 Blistering pattern and formation of nanofibers in capillary thinning of polymer solutions. *Physical review letters* **100** (16), 164502.

SAVVA, N. & BUSH, J. W. M. 2009 Viscous sheet retraction. *Journal of Fluid Mechanics* **626**, 211–240.

SEVILLA, A. 2011 The effect of viscous relaxation on the spatiotemporal stability of capillary jets. *Journal of Fluid Mechanics* **684**, 204–226.

STELTER, M., BRENN, G., YARIN, A. L., SINGH, R. P. & DURST, F. 2002 Investigation of the elongational behavior of polymer solutions by means of an elongational rheometer. *Journal of Rheology* **46** (2), 507–527.

SUI, C. & MCKENNA, G. B. 2007 Instability of entangled polymers in cone and plate rheometry. *Rheologica acta* **46** (6), 877–888.

SÜNDERHAUF, G., RASZILLIER, H. & DURST, F. 2002 The retraction of the edge of a planar liquid sheet. *Physics of Fluids* **14** (1), 198–208.

TANNER, R. I. 1970 A theory of die-swell. *Journal of Polymer Science Part B: Polymer Physics* **8** (12), 2067–2078.

TANNER, R. I. 2000 *Engineering rheology*, , vol. 52. OUP Oxford.

TANNER, R. I. 2005 A theory of die-swell revisited. *Journal of non-newtonian fluid mechanics* **129** (2), 85–87.

TAYLOR, G. 1959 The dynamics of thin sheets of fluid. iii. disintegration of fluid sheets. *Proceedings of the Royal Society of London. Series A, Mathematical and Physical Sciences* pp. 313–321.

TIRTAATMADJA, V., MCKINLEY, G. H. & COOPER-WHITE, J. J. 2006 Drop formation and breakup of low viscosity elastic fluids: Effects of molecular weight and concentration. *Physics of fluids* **18** (4), 043101.

VILLERMAUX, E. & CLANET, C. 2002 Life of a flapping liquid sheet. *Journal of fluid mechanics* **462**, 341–363.

VIRK, P. S. 1975 Drag reduction fundamentals. *AIChE Journal* **21** (4), 625–656.

ZELL, A., GIER, S., RAFAI, S. & WAGNER, C. 2010 Is there a relation between the relaxation time measured in caber experiments and the first normal stress coefficient? *Journal of Non-Newtonian Fluid Mechanics* **165** (19), 1265–1274.

ZHANG, G., ZHOU, J. S., ZHAI, Y. A., LIU, F. Q. & GAO, G. 2008 Effect of salt solutions on chain structure of partially hydrolyzed polyacrylamide. *Journal of Central South University of Technology* **15** (1), 80–83.